Multi-omics approach reveals dysregulated genes during hESCs neuronal differentiation exposure to paracetamol

Mari Spildrejorde[$,1,2,3], Athina Samara[$,4,5,*], Ankush Sharma[6,7,8], Magnus Leithaug[1,2,#], Martin Falck[1,8,§], Stefania Modafferi[2,+], Arvind Y. M. Sundaram[2], Ganesh Acharya[9,10], Hedvig Nordeng[1,11], Ragnhild Eskeland[1,7,14*], Kristina Gervin[**,1,11,12], Robert Lyle[**,1,2,13]

[$] Equal co-authorship contribution

[*] Corresponding author

[**] Equal co-authorship contribution

[1]PharmaTox Strategic Research Initiative, Faculty of Mathematics and Natural Sciences, University of Oslo, Norway

[2]Department of Medical Genetics, Oslo University Hospital and University of Oslo, Norway

[3]Institute of Clinical Medicine, Faculty of Medicine, University of Oslo, Oslo, Norway.

[4]Division of Clinical Paediatrics, Department of Women's and Children's Health, Karolinska Institutet, Sweden

[5]Astrid Lindgren Children's Hospital, Karolinska University Hospital, Stockholm, Sweden

[6]Department of Informatics, University of Oslo, Norway

[7]Department of Molecular Medicine, Institute of Basic Medical Sciences, Faculty of Medicine, University of Oslo, Oslo, Norway

[8]Department of Biosciences, University of Oslo, Norway

[9]Division of Obstetrics and Gynecology, Department of Clinical Science, Intervention and Technology (CLINTEC), Karolinska Institutet, Alfred Nobels Allé 8, SE-14152, Stockholm, Sweden.

[10]Center for Fetal Medicine, Karolinska University Hospital, SE-14186 Stockholm, Sweden.

[11]Pharmacoepidemiology and Drug Safety Research Group, Department of Pharmacy, University of Oslo, Norway

[12]Division of Clinical Neuroscience, Department of Research and Innovation, Oslo University Hospital, Oslo, Norway

[13]Centre for Fertility and Health, Norwegian Institute of Public Health, Oslo, Norway

[14]Lead contact

[#]Current address: Department of Analysis and Diagnostics, Section for Molecular Biology, Norwegian Veterinary Institute, Ås, Norway

[§]Current address: Department of Medical Genetics, Oslo University Hospital and University of Oslo, Norway

[+]Current address: Istituto di Genetica Molecolare, CNR - Consiglio Nazionale delle Ricerche, Pavia, Italy.

Correspondence: athina.samara@ki.se (A.S.) and ragnhild.eskeland@medisin.uio.no (R.E.)

Graphical Abstract

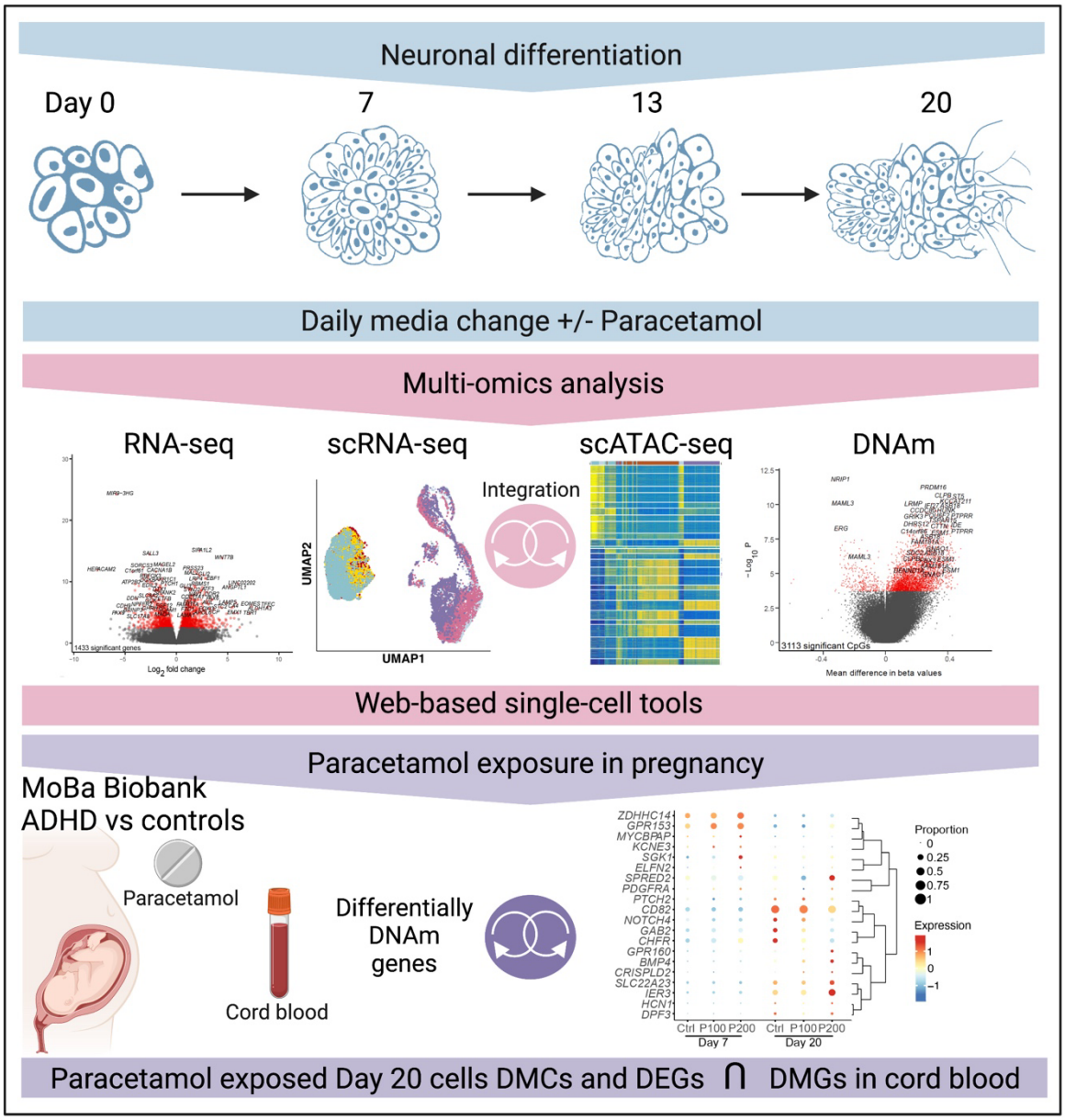

Created with Biorender.com.

Summary

Prenatal paracetamol exposure has been associated with neurodevelopmental outcomes in childhood. Pharmacoepigenetic studies show differences in cord blood DNA methylation between paracetamol exposed and unexposed neonates. However, causal implications and impact of long-term prenatal long-term paracetamol exposure on brain development remain unclear. Using a multi-omics approach, we investigated the effects of paracetamol on a model of early human brain development. We exposed human embryonic stem cells undergoing in vitro neuronal differentiation to daily media changes with paracetamol concentrations corresponding to maternal therapeutic doses. Single-cell RNA-seq and ATAC-seq integration identified paracetamol-induced chromatin-opening changes linked to gene expression. Differentially methylated and/or expressed genes were involved in signalling, neurotransmission, and cell fate-determination trajectories. Some genes involved in neuronal injury and development-specific pathways, such as *KCNE3*, overlapped with differentially methylated genes previously identified in cord blood associated with prenatal paracetamol exposure. Our data suggest that paracetamol may play a causal role in impaired neurodevelopment.

Keywords

Paracetamol; Acetaminophen; DNA methylation; multi-omics, single-cell RNA-seq, scATAC-seq, human embryonic stem cells, neuronal differentiation, telencephalic signatures, cord blood

Introduction

Paracetamol (also known as acetaminophen) is the most widely used analgesic and antipyretic during pregnancy, and it is considered safe for use as the first line option for pregnant women in need of mild analgesics or antipyretics[1–4]. A number of large epidemiological studies have reported an association between long-term maternal paracetamol use during pregnancy and increased risk of adverse neurodevelopmental outcomes, such as Attention Deficit/Hyperactivity Disorder (ADHD), in the child[5–13]. The association is reported to be stronger with long-term exposure and higher dose[14]. In 2019, the EUs pharmacovigilance safety committee (PRAC) reviewed all the available evidence, including non-clinical and epidemiological studies, regarding the impact of prenatal paracetamol exposure on impaired neurodevelopment in offspring. PRAC concluded that the available evidence is inconclusive, and recommended that the summary of product characteristics (SmPC) of paracetamol containing products should be updated to reflect the current state of scientific knowledge; "*Epidemiological studies on neurodevelopment in children exposed to paracetamol in utero show inconclusive results*" (PRAC, 2019)[15]. More recently, a group of researchers published a consensus statement and literature review in Nature Reviews Endocrinology concluding that there is growing evidence supporting the hypothesis that in utero exposure to paracetamol can impair fetal development[16]. This conclusion is still highly debated and contested by others (ENTIS, 2021)[17],[18,19] reflecting a need for further research.

Using samples from the Norwegian Mother, Father and Child cohort (MoBa) biobank, we have previously shown differences in DNA methylation (DNAm) in cord blood from children diagnosed with (ADHD) who have been exposed to paracetamol (>20 days) during prenatal development compared to unexposed children[20]. These findings suggest that DNAm might be involved in the pathogenesis of ADHD, but the causality and effect on neuronal differentiation and brain development is not known. It is well established that normal prenatal neurodevelopment involves cellular differentiation and establishment of cell-type specific epigenetic patterns, and that these events are prone to influences by environmental factors. For instance, maternal smoking has been shown to induce DNAm changes and modulate risk of neurodevelopmental

disorders (NDDs)[21–23]. If and how paracetamol modulates the apparent increased risk of NDDs is currently unknown.

Recently, we established a protocol for neuronal differentiation of human embryonic stem cells (hESCs), which can be used in neuropharmacological studies[24]. In the present study, we have used this model system of early human brain development and investigated the effects of paracetamol exposures on transcriptional and epigenetic regulation. Paracetamol doses were selected to reflect therapeutic maternal doses and fetal in utero exposures[25–27]. By integrating multiple omics methods (bulk RNA-seq, bulk DNAm, single-cell RNA-seq and ATAC-seq) we observed time and dose effects of paracetamol exposure during neuronal differentiation.

Results

Neuronal differentiation exposure, timeline, and morphology

We investigated epigenetic and transcriptomic effects of exposure to paracetamol using an in vitro neuronal differentiation protocol that drives hESCs towards anterior neuroectoderm[24,28]. The neuronal differentiation is divided into three stages: the neural induction phase (Stage I) ends at Day 7, the self-patterning phase (Stage II) ends at Day 13, and the FGF2/EGF2-induced maturation phase (Stage III) ends at Day 20 (**Fig. 1A**). We replaced culture media daily, and the cells were exposed to 100 or 200 µM paracetamol during differentiation from Day 1 and onwards. These concentrations have been documented to be in the range of therapeutic plasma concentrations[25–27]. Unexposed (control) and paracetamol-exposed cells were harvested for downstream analyses on Day 7 and 20. We also harvested control cells at the onset of differentiation (hESCs; Day 0), and on the intermediate timepoint that cells were passaged (Day 13) to assess whether paracetamol exposed cells had mRNA abundance changes related to proliferation or delayed differentiation.

The timeline of brightfield images of the control cells versus cells exposed to 100 (P100) or 200 µM paracetamol (P200) documents the morphological changes and cell culture density at differentiation Days 2, 4, 7, 8, 10, 13, 14, 17 and 20 (**Fig. 1B**). Tightly packed neuroepithelial cells form the neural rosettes by Day 7 reassembled at the next stage under high density cell passaging and proceeded to maturation. We did not observe any distinct morphological changes in the differentiating cultures exposed to 100 (P100) or 200 µM paracetamol (P200). However, preliminary paracetamol titration experiments showed that exposing the differentiating cells to 400 µM paracetamol increased cell death and unpatterned morphology in cells and were thus discontinued. A set of representative images following the 20-day timeline in control cultures and 100, 200 and 400 µM paracetamol-exposed cells is presented in supplemental information (**Fig. S1A-C**).

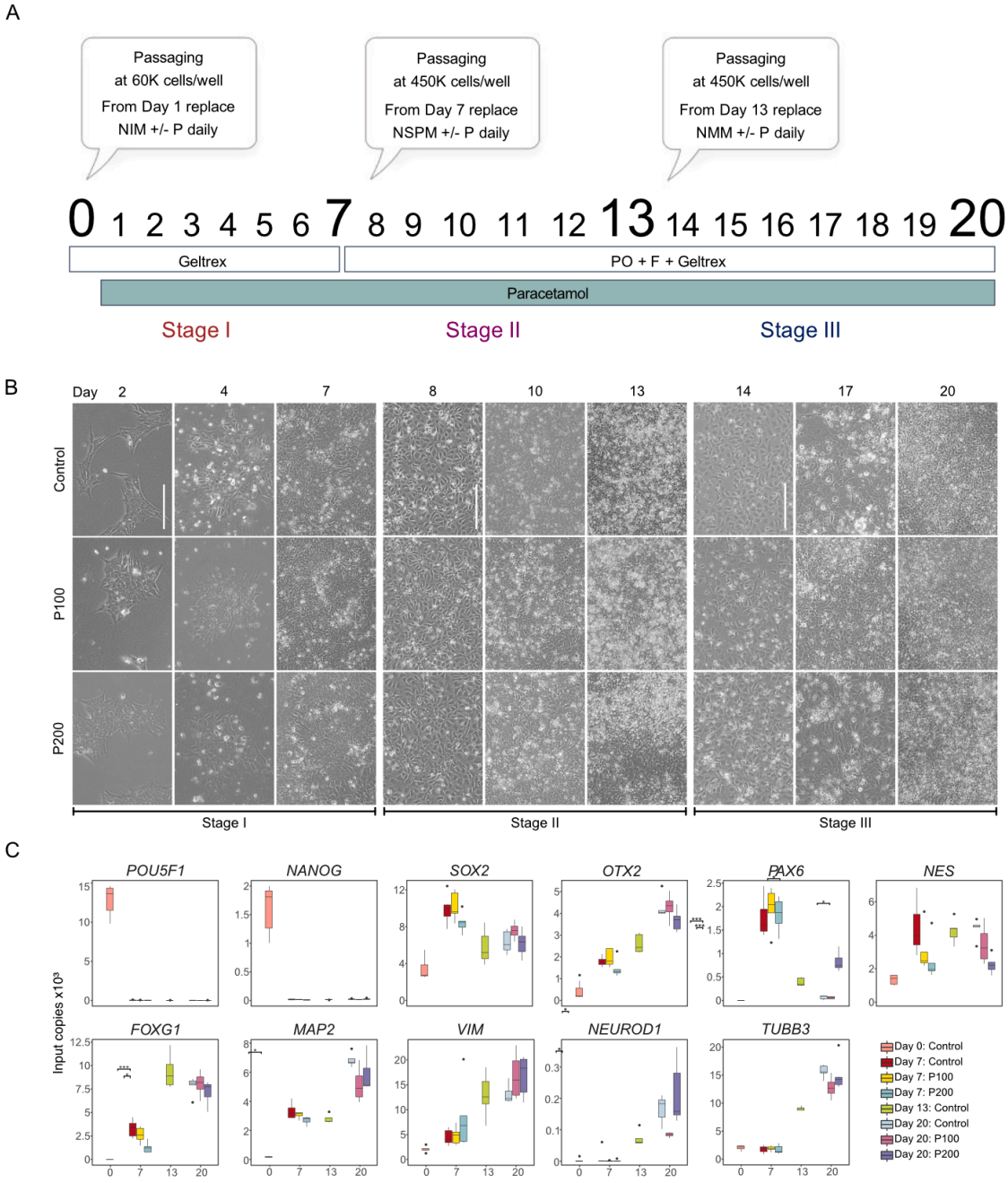

Figure 1. Neuronal differentiation of hESC to model neurodevelopmental effects of paracetamol.

A) Schematic illustration of the different phases of the neuronal differentiation protocol from Day 0 to Day 20. Cells were exposed to 100 or 200 µM paracetamol from Day 1 and onwards. The effect of paracetamol on gene expression and epigenetic profiles was evaluated at Day 7 and Day 20. B) Representative brightfield images of the differentiation timeline for control, P100 or P200 cells during differentiation at Day 2, 4, 7, 8, 10, 13, 14, 17 and 20 (scale bar corresponds to 100 µM). C) ddPCR results from 4-6 replicates of mRNA expression of selected marker genes from Days 0, 7, 13 and 20. Significant comparisons are marked with asterisks (Student's t-test, *: $p <= 0.05$, ***: $p <= 0.001$).

Validation of differentiation markers

The effect of paracetamol on gene expression was assessed at Days 7 and 20 was assayed using digital droplet PCR (ddPCR) (**Fig.1C**). Expression of the pluripotency transcription factors (TFs) *POU5F1* and *NANOG* decreased significantly after neural induction. As anticipated, we observed an increase in expression of the neural markers *SOX2, OTX2, FOXG1* and *MAP2* on Day 7 and *VIM*, *TUBB3* and *NEUROD1* on Day 13. Notably, the expression of *FOXG1*, *MAP2* and *NES* was significantly different between exposed and control cells on Day 7. Differential expression upon paracetamol exposure was also documented for filament *NES*, *PAX6* and *NEUROD1* on Day 20.

Paracetamol-induced gene expression changes in genes involved in neural development

To delineate the effect on gene expression, we performed bulk gene expression analysis using RNA-seq in controls and paracetamol exposed cells (P100 and P200; **Fig. 2**, **S2** and **Table S1**). Principal component analysis showed that samples clustered according to differentiation day (**Fig. S2A; STAR Methods**). Overall, when we compared P100 and control we identified 121 differentially expressed genes (DEGs, **Fig. 2A**) and 1 433 DEGs between P200 and control (**Fig. 2B**) from Day 7 to Day 20 (**Table S1**). Pairwise comparisons between paracetamol (P100 and P200) and control at each day are shown in **Fig. S2B-C**. The bulk RNA-seq analysis of the previously selected marker genes (**Fig. 1B**) correlated well with the ddPCR results of selected marker genes (**Fig. S1D**).

Gene set enrichment analyses (GSEA) analyses identified enrichment of downregulated BPs involved in synaptic organization, transmission, and regulation in the P100 time-response analysis (**Fig. 2C**). Notably, the upregulated BPs in the P200 time-response analysis were enriched for forebrain regionalization, cerebellar cortex formation and hindbrain differentiation (**Fig. 2D**). Also, the DEGs associated with P100 and P200 were enriched for common BPs reflecting enrichment of transmitter transport and regulation, synaptogenesis, synaptic organization, and plasticity.

The bulk RNA-seq pairwise comparisons of the P100 and P200 paracetamol-exposed cells to controls, showed an overlap of several DEGs (**Fig. S2D-F**). Exposure to paracetamol was associated with downregulation of genes previously linked to migration and neural development (e.g. *NTRK3*, *PMEL*[29], *CCDC184*[30], *MYT1*[31,32]). Furthermore, we identified DEGs linked to synaptic organization and transduction (e.g. *MYO16* [33], *HS3ST4* [34], *SORCS3* [35]), metabolism (*GCK* [36]), neuronal survival, dendrite branching, axonal growth and neural projection in development (e.g. *NSG1*[37], *TMEM3C6*[38], *TMOD1*[39], *PLPPR4*[40], *NEBL*[41], *NRN1*[42] and *GFRA2*[43]) and channelopathies (e.g. *CACNA1B/C*[44], *SCN3A*[45]) (**Fig. 2E**). Thus, these bulk RNA-seq analyses revealed transcriptional dysregulation of genes related to possible developmental delays between control and paracetamol-exposed cells.

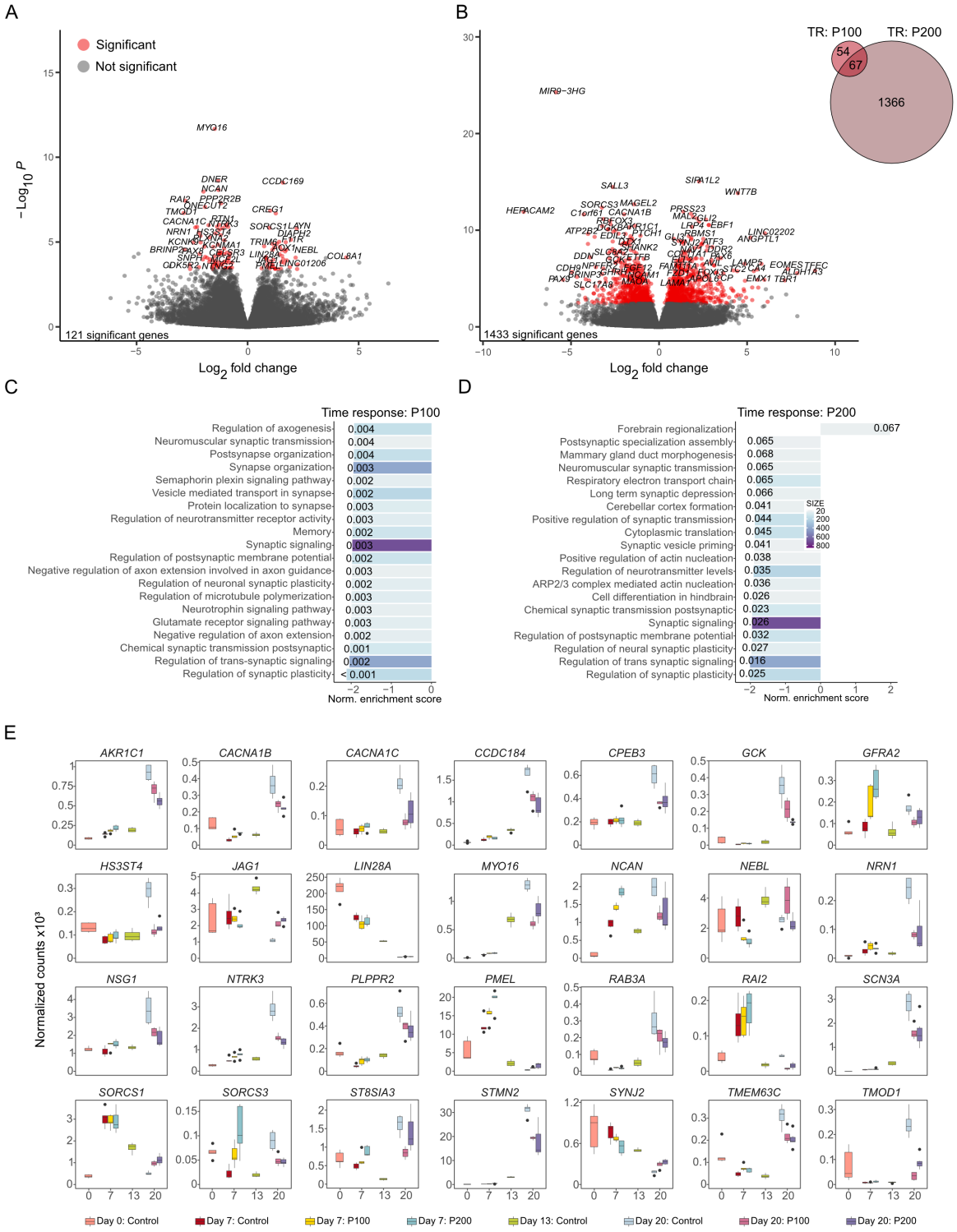

Figure 2. Paracetamol exposure of differentiating hESCs modulates expression of genes involved in neural development. Volcano plots of longitudinal differences in gene expression in A) P100 and B) P200 cells from Day 7 to Day 20. Corresponding Venn diagram shows the number of overlapping DEGs between the time-response (TR) of the two concentrations of paracetamol. Top 20 enriched BPs in C) P100 cells and D) P200 cells over time. E) Gene expression levels of selected DEGs, which overlapped between TR P100 and TR P200.

Single-cell RNA sequencing reveals dose-specific changes in several major cellular processes after paracetamol exposure

To explore cell-type specific gene expression and maturation signatures over time, we performed single-cell RNA sequencing (scRNA-seq) analysis of control and paracetamol-exposed cells (P100 and P200) at Days 7 and 20 (**Table S2**). Specifically, our aim was to determine whether paracetamol exposure caused deviations in neuronal differentiation compared to control cells. A total of 15 201 cells (n=6 924 Day 7 cells, n=8 277 Day 20 cells) from two time-course experiments were aggregated and projected in Uniform Manifold Approximation and Projections (UMAPs, **Fig. 3; STAR Methods**). The scRNA-seq data may also be visualized in the open access webtool (**hescneuroparacet**), where expression of genes can be explored per cell, cluster, and time point.

The cells clustered according to differentiation day and not exposure to paracetamol (**Fig. 3A**). Consistent with previous results[28], seurat-predicted cell cycle phase showed an increase in G1 cells at Day 20 (**Fig. 3B**). However, the existing cell cycle analysis tools are unable to decipher the proportion of neurons that are in G0 phase. Using CytoTRACE pseudotime differentiation trajectory analysis, the most differentiated cells were found at Day 20 (**Fig. 3C**). The composite neuronal differentiation P1-P13 clusters were manually annotated with genes *CRABP1*, *PAX6, TYMS, KIF20A, FGF17, HES5, WNT5A, ASCL1, GNG8, DLX1, SRSF9, VEPH1* and *TAGLN2*, respectively (**Fig. 3D**). At Day 7, we observed a subtle shift in cell composition from P1 to P2 in the cells exposed to paracetamol (**Fig. 3E)**. The effect was more prominent at Day 20 with a higher proportion of paracetamol-exposed cells compared to controls annotated to cluster P5 and a more prominent effect at P200 exposure, whereas a lower proportion were annotated to P6, P9 and P10 for both concentrations (**Fig. 3E**).

To further investigate cell identity, the data were juxtaposed with a scRNA-seq Human Brain dataset[46] (**STAR Methods**). Most cells at Day 7 were resembled neuronal progenitors, whereas cells at Day 20 were similar to neuronal progenitors, neuroblasts and neurons (**Fig**. **3F**). At Day 20, there was a subtle shift from cells annotated as neuroblasts towards the less differentiated neuronal progenitors in paracetamol-

exposed cells compared to controls (**Fig**. **3G).** UMAP plots of the dual co-expression of the genes *ID2/ID4*, *CDK1/CDKN1C*, *HES1/STMN2, REST/NEUROD1, NKX2-1/WNT7B* and *NTRK1/DLX6-AS1* indicate agreement between these maturation signatures and the CytoTRACE trajectory analysis (**Fig. 3C** and **H**).

The analysis of the top DEGs per cluster (**Fig. S4**) and data exploration (**Fig. S5)**, showed that paracetamol exposure induced changes in several major processes at the selected timepoints. We identified dose-dependent changes that link paracetamol exposure to cell-cycle transition important in neuronal maturation (*MKI67, PCNA, TP53*, *CDK1, MYBL2* and *GJA1)* neural induction differentiation, or its inhibition (*REST, RAX, PAX6, HES1, HES5, ID3* and *ID4),* neurite outgrowth and cortical neurogenesis (*GBA2, ASPM*), neuronal maturation *(CDKN1C, POU2F1, POU3F1, ROBO1, STMN2* and *STMN4)* and WNT and FGF signalling (*FRZB, WNT4, WNT7B, FGF8* and *FGFRL1)* (**Fig. S5)***.* We observed a differential and dose dependent expression of crucial spatiotemporally regulated transcription factors associated with brain development (e.g., *NKX2.1, OTX2, FOXG1, ASCL1, ISL1, EMX2* and *HOXA1*), neurotransmitter transporter expression (*SAT1*, *SLC2A1*)*.* Finally, we found differential expression of genes related to cellular response to toxic insults (e.g., *DDR1*; **Fig. S5)***.*

Paracetamol exposure is associated with differential expression of neural lineage markers

To extract the biological significance and interpretation of DEGs after paracetamol exposure in the scRNA-seq datasets, we performed GO analyses and identified enrichment of GO terms and BPs. First, we identified the top 10 upregulated and downregulated BPs between control cells and P100 (**Fig. S3A**) or P200 cells (**Fig. S3B**) on Day 7. Notably, BPs involved in *DNA replication* and *cell-cycle regulation* were upregulated in cells exposed to both paracetamol doses, and a downregulation of a BP which involves *generation of neurons*. DEGs in P100 cells compared to control cells were enriched for more neuronal specific annotations. Furthermore, P200 compared to control cells identified upregulated GO terms involved in cellular responses to toxic insults and *DNA checkpoint activation*. The top 20 DEGs between P100 (**Fig. S3C**) or P200 (**Fig. S3D**) and control cells at Day 7, are shown as bubble

plots of relative gene expression. The gene expression of the top overlapping genes between the P100 and P200 cells compared to control cells at Day 7 (**Fig. S3E**) extends the GO annotations to gene specific similarities. We identified changes in crucial genes, such as the master gene of forebrain development *FOXG1*[47] and genes of the *HES* and *ID* gene families involved in differentiation and neurogenesis[48].

Next, we extracted the top 10 upregulated and downregulated BPs among the DEGs between control cells and P100 (**Fig. S3F**) or P200 cells (**Fig. S3G**) on Day 20. In both comparisons, downregulated GO terms included *neuron/nervous system developmen*t and *microtubule polymerization or depolymerization*. Of the top 20 DEGs at Day 20 between paracetamol-exposed and control cells, we found major patterning TFs, such as *NKX2-1* and *EMX2* (**Fig. S3H-I)**. Moreover, genes that belong to the ZIC family, among other genes involved in Notch and Wnt signalling, were also identified (**Fig. S3H-I)**. The gene expression of the top overlapping genes between P100 and P200 cells were compared to control cells at Day 20 (**Fig. S3J**). The analysis of GO terms delineated gene specific changes, such as upregulation of *SELENOW* (**Fig. S3D**), previously associated with neuroprotection from oxidative stress[49]. The paracetamol-induced differentiation lag as evidenced by the *PAX6* expression in the P200 cells (**Fig. 1C**). We also observed a downregulation of tissue- and stage-specific genes, such as *FABP7*, *ISL1, STMN2* and *INA*. In addition, *TUBB1A*, the isotype associated with postmitotic neurons[50], and *TUBB2B*, that constitutes 30% of all brain beta tubulins[51], were also found among the downregulated genes. Interestingly, *PEG10* and *C1orf61* and *MIR9-1HG* appear in the Day 20 P200 comparisons, genes which have recently been linked to cortical migration and intercellular communication[52], further documenting how the P200 dose of paracetamol could affect proper network formation and cell-to-cell signalling.

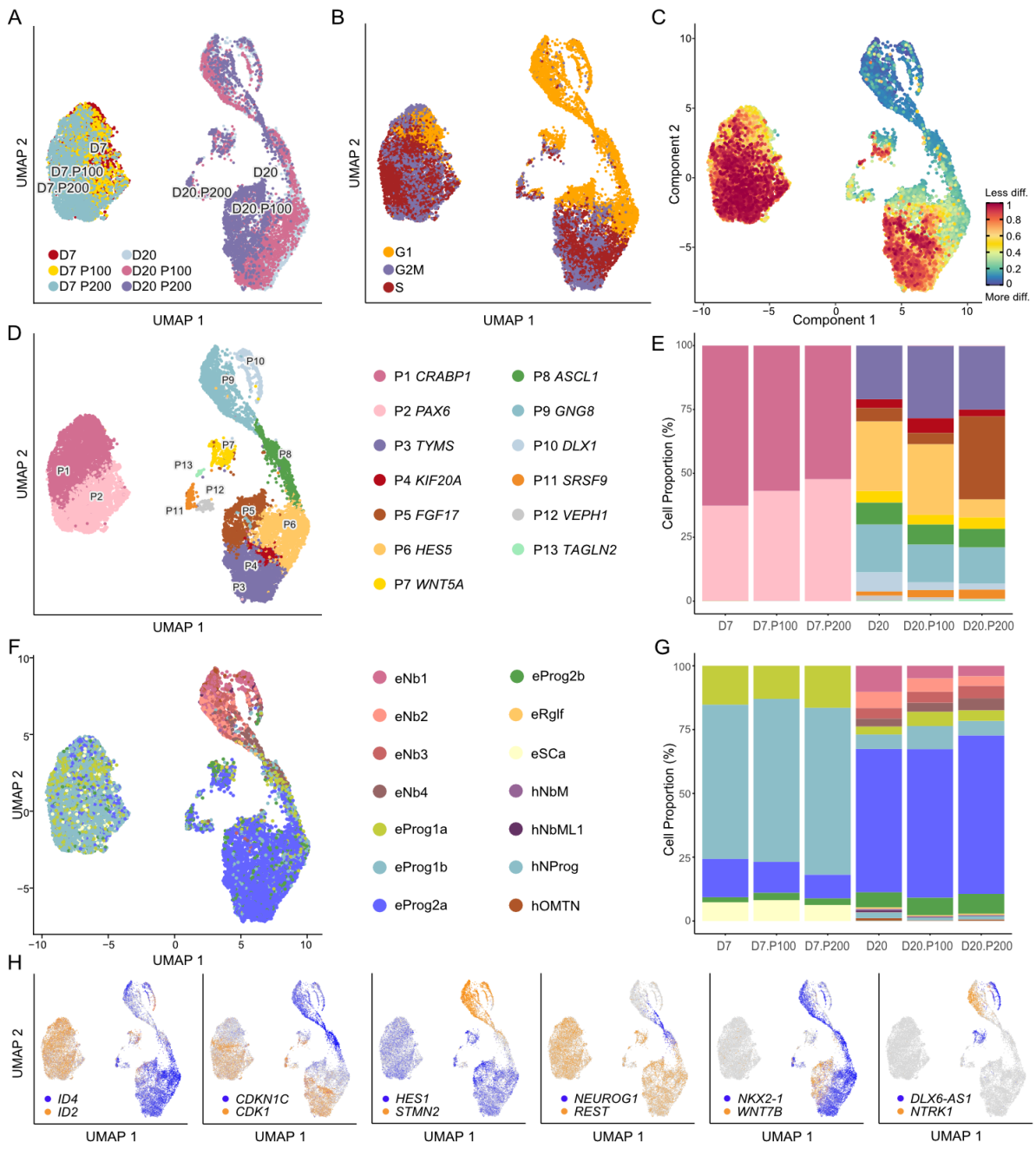

Figure 3. scRNA-seq analysis revealed shifts in cell type composition of differentiating cells exposed to paracetamol. Day 7 and Day 20 control cells and cells exposed to 100 μM (P100) or 200 μM (P200) paracetamol were visualized with UMAP and coloured by A) sample identity, B) Seurat predicted cell cycle phase, C) CytoTRACE pseudotime differentiation trajectory, D) defined Seurat clusters at resolution 0.4 with corresponding gene annotations and E) cell proportions per cluster. F) UMAP plots of cells coloured by SingleR cell annotation to Human Brain reference with corresponding cell annotations. Cell types starting with "e" are hESC derived cells and cell types starting with "h" are in vivo human embryo cell types. Nb1-4; neuroblasts, Prog1-2; neuronal progenitors, Rglf; radial glia-like cells, SCa; stem cells, NbM; medial neuroblasts, NbML1; mediolateral neuroblasts, NProg; neuronal progenitors, OMTN; oculomotor and trochlear nucleus.

G) Corresponding cell proportions per cell type. H) UMAP plots of dual gene coexpression for *ID2/ID4*, *CDK1/CDKN1C*, *HES1/STMN2, REST/NEUROD1, NKX2.1/WNT7B* and *NTRK.1/DLX6-AS1* indicate that maturation signatures agree with the CytoTRACE trajectory analysis.

Integration of scATAC- and scRNA-seq link paracetamol-induced changes in chromatin opening to transcriptional activity at Day 20

To understand whether paracetamol exposure during differentiation influenced the chromatin landscapes at Day 20 we performed scATAC-seq. We obtained 3 042 nuclei for Day 20 control and 3 480 and 4 282 nuclei for Day 20 exposed to 100 µM (P100) and 200 µM paracetamol (P200), respectively. First, we reanalysed scRNA-seq data from Day 20 controls, P100 and P200, and remapped the P3-P13 clusters (**Fig. 4A-B**). The maturation trajectory cohered with the initial Day 7-Day 20 time point analysis (**Fig. 4C and 3C**). Next, we mapped the scATAC-seq data (**Fig. 4D**) to 15 scATAC-seq clusters (C1-C15; **Fig. S6A**) that we integrated with the annotated scRNA-seq P3, P5, P9, P10 and P13 clusters (**Fig. 4E)**. The quality of the combined scATAC-seq datasets was documented with an even distribution of integrated clusters (P3, P5, P9 and P10) over TSS, promoters, exons, introns, and distal genomic regions (**Fig. S6B-C**). The P13 cluster is represented by very few nuclei and displayed lower enrichment across all genomic regions.

To further explore the differential chromatin accessibility across the genome, we correlated distal accessible regions with gene expression[53]. This allows for identification of putative cis regulatory elements (CREs) for biological and functional comparisons of Day 20 control cells with P100 and P200 exposed cells. We grouped the peak-to-gene links (P2GLs) into five clusters and plotted heatmaps of gene expression and gene scores for all three datasets (P2GLs represent potential genes linked to chromatin opening, **Fig. 4G-I**). We observed relatively similar numbers of putative CREs in controls (n=30 771), P100 (n=26 216) and P200 (n=28 883). Notably, the heatmaps of controls and P100 and P200 cells were different with an absence or presence of the integrated cluster P5, also described as having differential prominence in the scRNA-seq data (**Fig. 3E**). Only 6 960 of the putative CREs overlapped between the three datasets, whereas 4 732, 3 435 and 6 534 putative CREs specifically

overlapped between control and P100, control and P200, and P100 and P200, respectively (**Fig. 4J** and **Table S3A-C**). Moreover, we observed that many of the putative CREs were only detected in individual datasets (Day 20 control; n=15 644, P100; n=10 460 and P200; n=12 304 CREs). These variations in putative CREs suggests that paracetamol exposure results in changes in chromatin accessibility. For example, in the locus of the neuronal marker gene *STMN2,* which showed higher gene expression in unexposed cells compared to exposed cells, showed changes in chromatin opening peaks in paracetamol exposed cells (**Fig. S6D, S3J** and **S5**). Furthermore, accessibility peaks in the *ELAVL4* locus displayed differential chromatin opening in clusters P3, P5, P9 and P10. We also identified putative CREs in the exposed cells that correlated with higher *ELAVL4* expression in control cells compared to P100 or P200 cells (**Fig. 4K** and **Table S3A-C)**.

Paracetamol affects region-specific chromatin accessibility

The putative enhancer-gene interactions identified likely represent chromatin regulomes in the control and the paracetamol-exposed cells. We therefore compared the level of overlap of linked genes to better understand the effect of paracetamol exposure on chromatin regulation. A larger proportion of linked genes overlapped between the Day 20 control and paracetamol exposed cells (n=4 047), and the P100 (n=1 224) and P200 (n=1 048) cells (**Fig. 4L** and **Table S3A-C** and **V**). GO analyses of the linked genes revealed a common enrichment of BPs, such as *nervous system development*, *biological regulation, neurogenesis,* and *neuron differentiation*, varying in the different k-means (km) clusters (**Fig. S6D** and **Table S3D-F**). Linked genes identified in paracetamol exposed cells (P100, n = 652; P200, n = 915 and 1424 for both P100 and P200) indicate exposure-induced changes in gene expression. Interestingly, linked genes including neuronal lineage transcription factors (e.g. *PAX6*, *NEUROD4, NEUROG1*, *SOX9* and *SOX2*) and genes involved in chromatin modification (e.g. histone H3K27 acetyltransferase *EP300*[54], Histone H3K27me3 demethylase *KDM6A*[55] and chromatin remodeller SNF2 subfamily member *SMARCAD1*[56]), suggest that paracetamol may contribute to modulation of transcriptional regulation and chromatin structure (**Table S3V**). In addition, GO analysis of the putative CREs identified enrichment of BPs per k-means group and

sample are shown in **Tables S3G-U**.

Enriched TF motifs in the CREs may infer gene expression program regulation. We identified TFs (n=29) that were common for control, P100 and P200 cells, including *NEUROD1, NEUROG1, SOX9, HMGA1* and members of the ONECUT and NHLH families, which have previously been described in the neuronal differentiation protocol[28]. TFs that were common between P100 and P200 cells (n=18) or dependent on paracetamol dose (**Fig. 4M-N, S3I, S5, S6F** and **Table S4**). The TF footprint per cluster and motif enrichment and computed sequence logos for *OTX2, TBR1* and *EMX2* show that these factors are enriched and potentially regulate genes in these integrated clusters (**Fig. 4O)**.

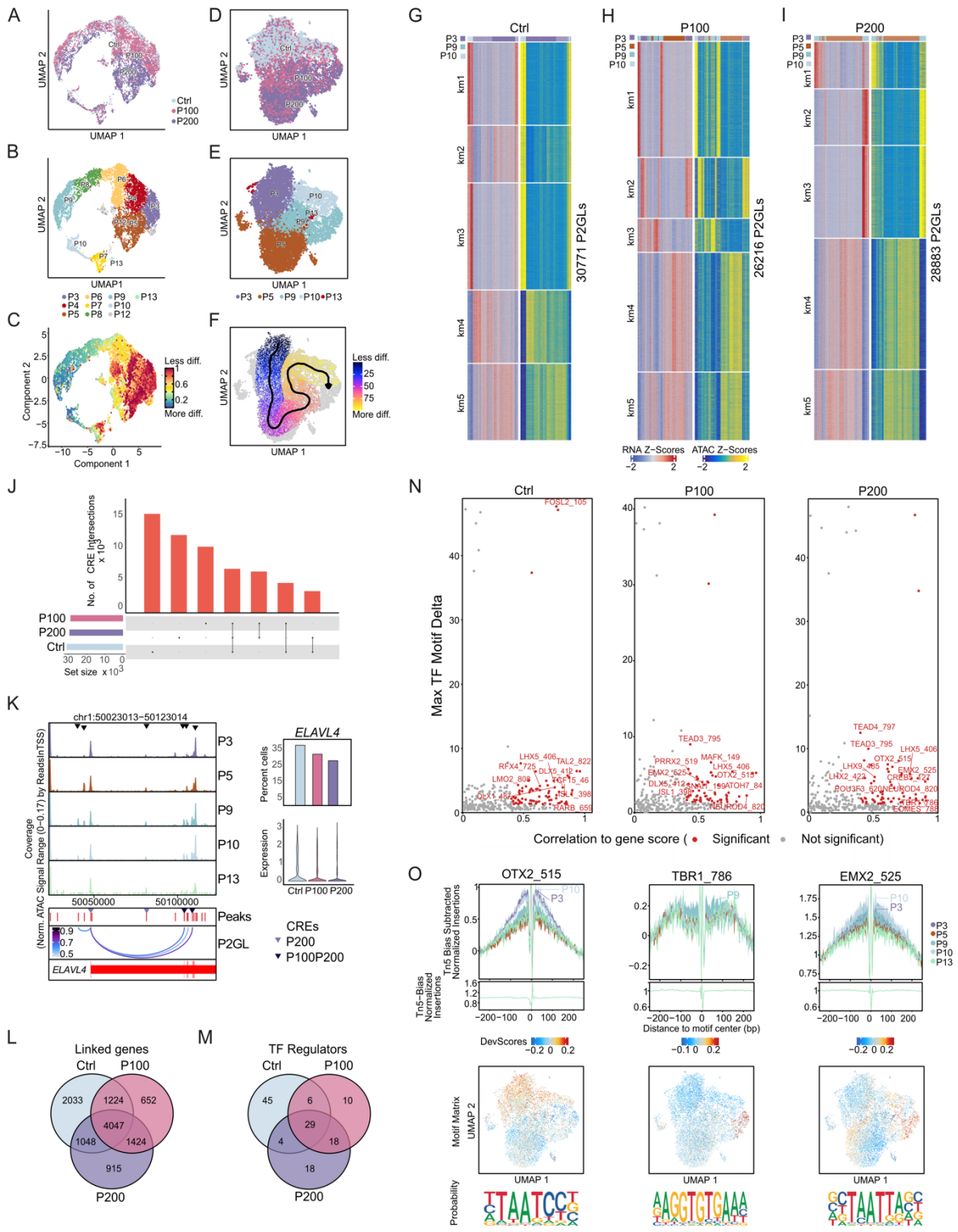

Figure 4. Effects of paracetamol on chromatin accessibility and integration with scRNA-seq at Day 20.

A-C) scRNA-seq UMAP plots coloured by A) sample identity, B) scRNA-seq clusters or C) CytoTRACE pseudotime differentiation trajectory. D-E) scATAC-seq UMAP plots of coloured by D) sample identity and E) remapped clusters following constrained alignment of cell populations by scATAC-seq and scRNA-seq integration. F) Supervised pseudotime trajectory of integrated

clusters. G-I) Heatmaps of scATAC-seq and scRNA-seq side-by-side representing peak to gene links (P2GLs) in G) control cells, H) P100 cells and I) P200 cells. Rows were clustered using k-means (k = 5). J) Overlap of putative CREs from P2GLs analyses of Day 20 control versus P100 and P200. K) *ELAVL4* locus browser view (GRCh38.p13) from 5000 cells with ATAC-seq signals in integrated clusters. Differential chromatin opening (black triangles), ATAC peaks (red), P2GLs (arcs) and putative CREs enriched in P200 or P100 and P200 cells (coloured triangles) are shown. The bar plot to the right shows the corresponding percentage of cells expressing *ELAVL4*, and the plot below represent the expression levels. L) A Venn diagram representing overlap of linked genes. M) Venn diagram of TF regulators identified from P2GLs integrative analysis. N) A selection of positive TF regulators computed using gene integration scores with motifs in the putative CREs. O) Footprints for selected TF regulators OTX2, TBR1 and EMX2 demonstrating preferential opening per cluster; below are the corresponding ArchR motif deviation scores, motif matrix and representative sequence logos identified in the scATAC-seq dataset.

Paracetamol induced changes in DNAm during neuronal differentiation

To assess whether exposure of hESCs undergoing neuronal differentiation to paracetamol induced DNAm changes, we analysed control cells and cells exposed to 100 (P100) and 200 µM paracetamol (P200) at Day 7 and 20. The experimental set-up included analysis of control cells harvested at Day 0 and 13 as reference points of possible dysregulation (**Fig. 5** and **S7, Table S1**). Assessment of principal component analysis showed clustering of samples according to differentiation day (**Fig. S7C; STAR Methods**). Overall, the distribution of DNAm was indistinguishable across exposed and control cells at all time points regardless of paracetamol dose (**Fig. S7A**). In contrast, non-CpG DNAm levels decreased during differentiation and were lower in cells exposed to 200 µM paracetamol compared to control cells at Day 20 (**Fig. S7B**).

To investigate whether the cells exposed to different doses of paracetamol (P100 and P200) respond differently than control cells from Day 7 to Day 20, we performed a DNAm time-response analysis. We observed no significant DNAm changes in P100 compared to control between Day 7 and Day 20 (not shown). In contrast, 3 113 CpGs responded differently to P200 compared to control cells over time (**Fig. 5A**). CpGs showing an increase in DNAm are annotated to genes with key functions in dynamic cellular redox changes in the developing brain, such as the neural specification gene *PRDM16*[57] enriched for GO terms such as synaptic signalling and chemical synaptic

transmission (**Fig. 5B**). CpGs showing a decrease in DNAm are annotated to genes enriched for gene ontology (GO) terms involved in synaptic regulation, GABAergic signalling, and cell morphogenesis (**Fig. 5B**). Overall, when we assessed DNAm levels at all CpGs (**Fig. 5C**) compared to all significant CpGs (**Fig. 5D**), we found a general dose-dependent increase in DNAm levels at significant sites in paracetamol-exposed cells compared to controls at both Day 7 and Day 20. The annotation of differentially methylated CpGs (DMCs) in relation to genes and CpG islands was similar across the different comparisons (**Fig. S7D-E**).

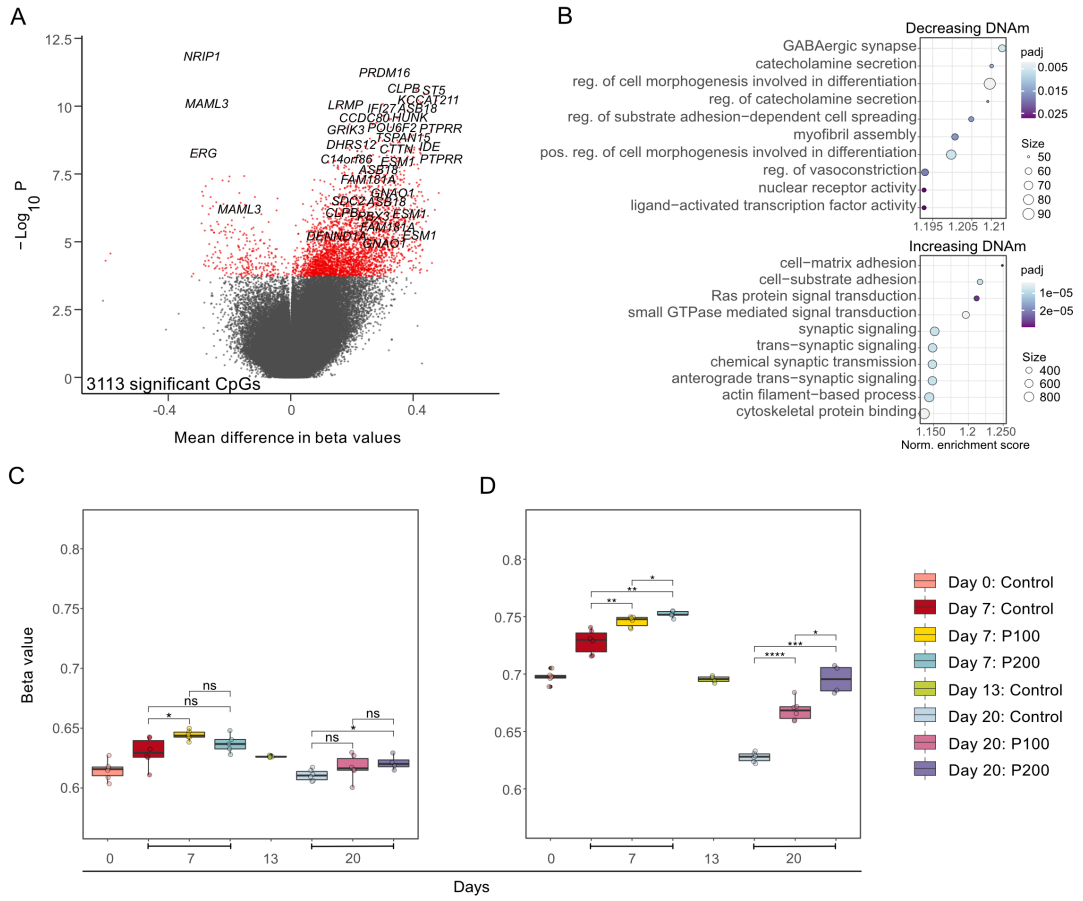

Figure 5. Exposure to paracetamol induces changes in DNAm over time during neuronal differentiation.

A) Volcano plot showing the effect of 200 µM paracetamol from Day 7 to Day 20. CpGs with adjusted p-value < 0.05 were considered significant. B) Corresponding enriched GO-terms for CpGs showing a decrease in DNAm (top) or an increase in DNAm (bottom) over time (Day 20 – Day 7) in P200 cells compared to control cells. C) Average DNAm levels per sample for all CpGs across differentiation for Day 0, 7, 13, and 20. D) Average DNAm levels per sample for all significant CpGs (paracetamol-exposed cells vs control comparisons) at Day 0, 7, 13, and 20. E-F) *p < 0.05, **p < 0.01, ***p < 0.001, ****p < 0.0001.

Next, we performed comparisons of DNAm levels in paracetamol-exposed cells to controls at Day 7 (**Fig. S7F and H**, **Table S1**) and Day 20 (**Fig. S3G and I**, **Table S1**) for the different doses. As expected, we observed more significant DNAm changes after longer exposure (Day 20) and at higher concentration of paracetamol (P200) (**Table S1**). We found no dose-dependent DMCs at Day 7 whereas at Day 20 a larger number of CpGs (n=8 940) were differentially methylated between P100 and P200. Moreover, there was some overlap between DMCs at 7 and Day 20 (**Fig. S7J**). To define a regulatory role of paracetamol induced DNAm changes on gene expression, we assessed the overlap between DEGs and differentially methylated genes (DMGs) for the pairwise comparisons and time response analyses (**Table S1**). The percentage of DMGs overlapping with DEGs varied between 3 and 63 % for the different comparisons. The P200 time response analysis revealed 180 overlapping genes, and some selected genes are visualized in **Figure 6**. DNAm levels for *GRIK3*, *CACNA1D*, *ABAT*, *MAPT* and *ANKRD6* were inversely correlated with gene expression, whereas DNAm levels for *PAX7*, *CDH2* and *WNT7B* were positively correlated with gene expression at Day 20. *GLI3* had DNAm levels that correlated with both negative and positive regulation (**Fig. 6**).

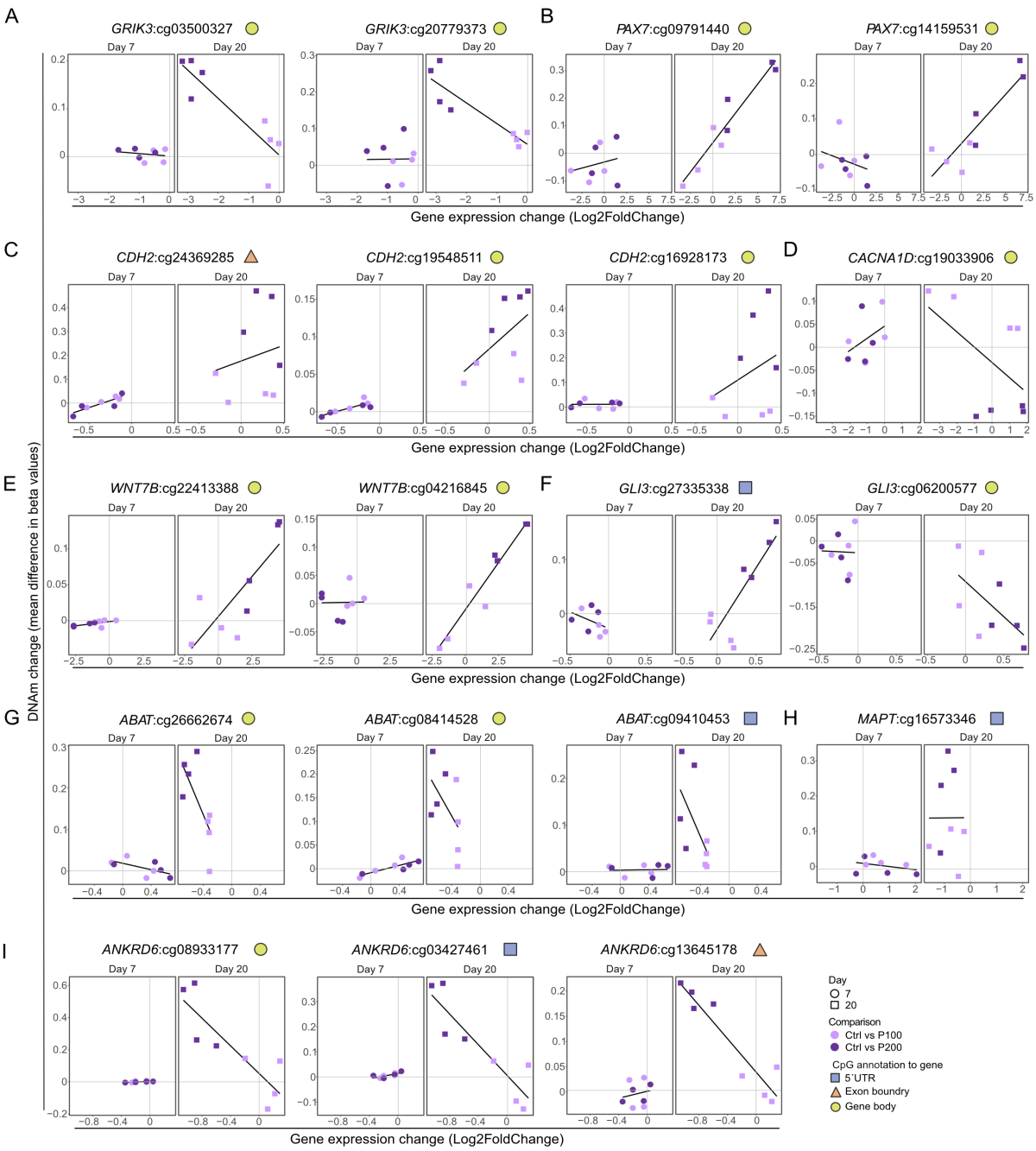

Figure 6. DNAm and gene expression for selected overlapping DMCs and DEGs. Change in DNAm and gene expression levels between control and P100 or P200 for A) *GRIK3*, B) *PAX7*, C) *CDH2*, D) *CACNA1D*, E) *WNT7B*, F) *GLI3*, G) *ABAT*, H) *MAPT* and I) *ANKRD6*. Each point represents a matched replicate between RNA-seq and DNAm and black lines represents a linear regression line of the mean of values.

Overlap of dysregulated genes in differentiating hESCs and cord blood from children exposed to paracetamol during pregnancy

We have previously identified an association between differential DNAm in cord blood and long-term paracetamol exposure during pregnancy in children with ADHD[20]. To assess the translational potential and causality of these findings, we compared the dysregulated genes identified in the present model to the differentially methylated genes associated with paracetamol exposure in cord blood. In brief, the DMCs and the DEGs in paracetamol-exposed differentiating cells at Day 20 were correlated with DMGs in cord blood[20]. Interestingly, we identified an overlap of 20 genes between DEGs and DMCs for P100 and P200 in differentiating hESCs and differentially methylated genes identified in cord blood between paracetamol-exposed children with ADHD versus controls (**Fig. 7A**) and only one gene (*KCNE3*) with paracetamol-exposed children with ADHD versus ADHD controls (**Fig. 7B**).

We assessed the expression of these 20 overlapping genes in scRNA-seq data (**Fig. 7C**) and RNA-seq data (**Fig. 7D**). Notably, genes involved in differentiation, such as *GAB2*[58]*,* or *Notch and Hedgehog signalling pathways* (for example, *NOTCH4*[59], *PTCH2*[60] *SHISA2*[61]) show a dose-dependent downregulation of expression in paracetamol-exposed cells compared to controls. This high variation in expression levels after paracetamol exposure compared to controls, indicates a dose effect. Among genes identified in Day 7 P200 cells, we observed upregulation of *ZDHHC14*[62] and *SGK1*[63], that are associated with control of neuronal excitability and neuronal response to injury, respectively. Several toxic insult response genes were also upregulated at Day 20 in the P200 treated cells, such as *IER3*[64], *SPRED2*[65], *GPR130*[66], and *SLC22A23*[67].

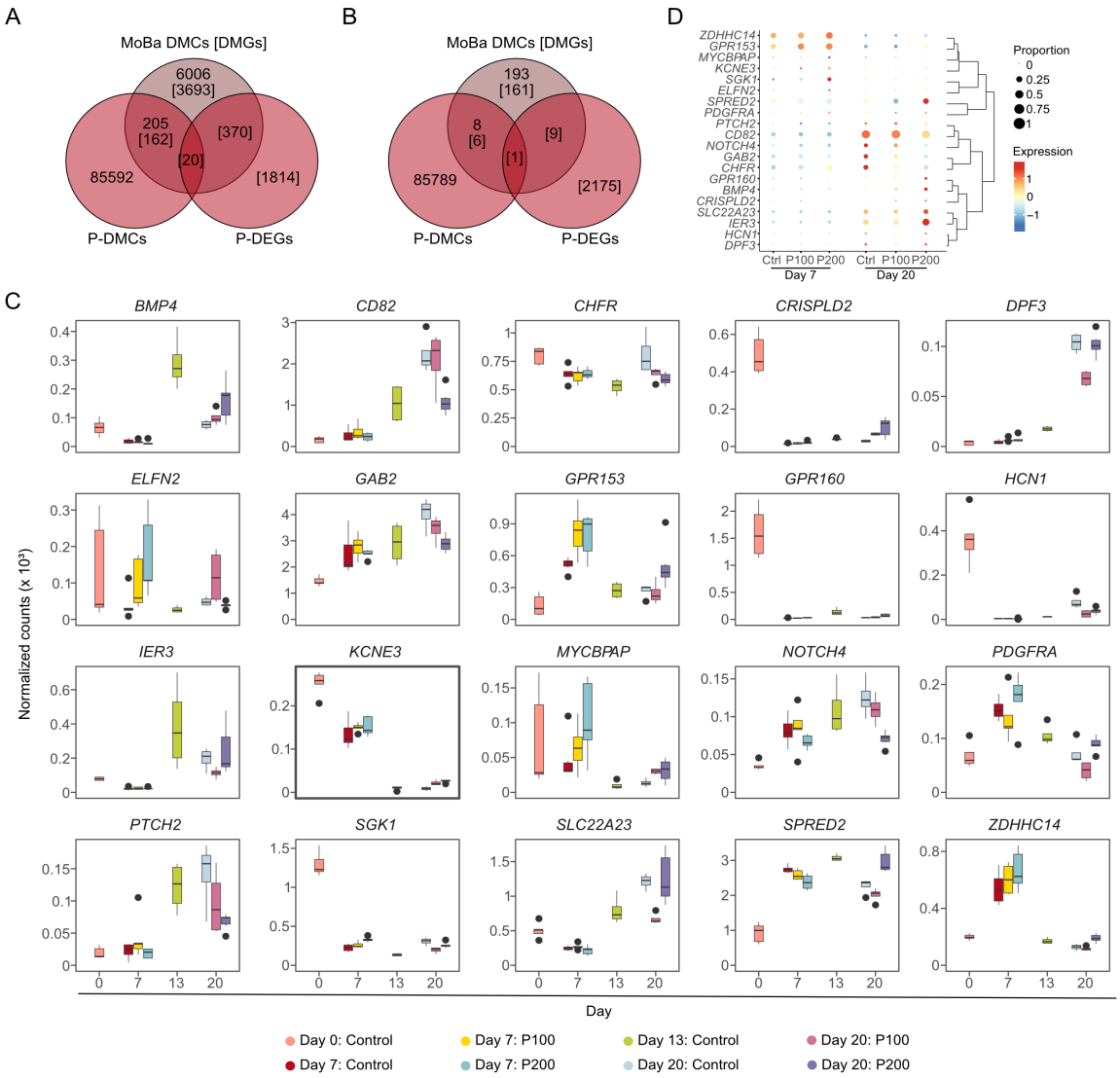

Figure 7. Overlap with differentially methylated genes in cord blood. A-B) Venn diagrams showing the overlap between DEGs and DMCs for P100 and P200 and A) paracetamol-exposed children with ADHD versus controls and B) paracetamol-exposed children with ADHD versus ADHD controls in cord blood. C-D) Gene expression levels of overlapping genes identified in cord blood derived from C) RNA-seq and D) scRNA-seq data.

Discussion

To our knowledge, this is the first multi-omics study investigating how paracetamol exposure affects epigenetic and transcriptional programmes involved in early brain development using an in vitro hESC model of neuronal differentiation[28].

We identified differential expression of genes enriched for BPs involved in transmitter transport and regulation, synaptic organization and synaptogenesis and plasticity. Interestingly, in cells exposed to the high dose of paracetamol (P200), we also identified enrichment of GO categories reflecting possible patterning deviations from forebrain differentiation. Thus, we observe an effect of paracetamol exposure on transcriptional dysregulation and possible developmental delays during neuronal differentiation. Additionally, among the common DEGs, irrespective of paracetamol dose, we identified *SORCS3,* which encodes a brain-expressed transmembrane receptor associated with neuronal development and plasticity that has been previously identified in a GWAS meta-analysis of ADHD significant risk loci[68]. The scRNA-seq analysis identified dose-dependent DEGs involved in several major processes during neuronal differentiation. Exposure to paracetamol resulted in a subtle shift in cell populations from P1 to P2 at Day 7. At Day 20 the P6, P9 and P10 clusters decreased whereas P5 markedly increased in P200. The DEGs link paracetamol exposure to genes involved in cell-cycle length and phase transition and genes important for neuronal maturation, neurite outgrowth, cortical neurogenesis, expression of neurotransmitter transporters, neuronal maturation and WNT and FGF signalling. Further, the data also documented dose-dependent differential expression of crucial spatiotemporally regulated TFs associated with brain development. These findings provide evidence of transcriptomic dose-dependent effects of paracetamol exposure related to cellular response to toxic insults and fate-determination deviation queues at the Day 20. Furthermore, the results identified an impact of paracetamol exposure on the regulation of central, autonomic and sympathetic nervous system development, which are all central to finetuning human cognition and associated with ADHD[69–71].

To further characterize and investigate epigenetic mechanisms involved in altered cellular heterogeneity and differentiation, we performed scATAC-seq to map CREs and compare the chromatin landscape changes between control and cells exposed to

P100 and P200 at Day 20 (**hescneurodiffparacet**). Interestingly, the results from these analyses identified differences in several chromatin accessible regions in genes previously associated with fate mapping and neurogenesis, which have been identified in risk determination studies focusing on cognition and autism spectrum disorders (e.g. *DLK1, DIO3, IPW* [72,73]) and ADHD (e.g. *MEG3*[74]).

Genome-wide association studies (GWAS) suggest that cognitive disorders might also result from the cumulative effect of gene variant regulation and parent-of-origin effect[74], which in ADHD has been associated with genes such as *DDC, MAOA, PDLIM1* and *TTR*. We also identified chromatin openness differences related to genes identified in the paracetamol exposed cells. For example, *PCDH7*, which acts as a cue for axonal guidance via roles in cell adhesion, was among the genes that were both differentially expressed and had different chromatin openness in Day 20 P200 cells. Dysregulation of *PCDH7* could be relevant to the semaphorin-plexin signalling documented by the enriched BPs in the P100 cells, and it is noteworthy as it has also been associated to ADHD[68].

We also identified dose-dependent differences in chromatin accessibility of the neural specification gene locus *PRDM16*, which correlates well with DNAm analyses where exposure to paracetamol was associated with increased DNAm at CpGs annotated to *PRDM16*. This gene has been linked to regulation of transcriptional enhancers activating genes involved in intermediate progenitor cell production and repressing genes involved in cell migration[57]. The molecular mechanism of *PRDM16* remains unknown but has been associated with reactive oxygen species regulation in the embryonic cortex[75].

Integrative analyses of scRNA-seq and scATAC-seq to explore the links between chromatin accessibility and gene expression documented high correlation and showed an overlap between scATAC-seq and scRNA-seq cell clusters. This analysis identified novel putative CREs, and linked genes affected by paracetamol exposure. Although a portion of linked genes overlapped between the control and exposed cells, there was only a small overlap between the putative CREs. This suggest that many local changes in chromatin opening were affected by paracetamol exposure and that these CREs may regulate different gene expression programmes in control and paracetamol

exposed cells. How paracetamol regulates chromatin opening is not known, and we have limited knowledge on the effect of paracetamol on the TFs recognition of DNA motifs. However, our data suggest that genes linked to putative CREs that were affected by paracetamol exposure have a role in regulation of transcription and chromatin. In particular, a linked gene specific for paracetamol exposure was *EP300*, which codes for a histone acetyltransferase responsible for the active enhancer mark H3K27ac[76]. *EP300* expression decreased subtly upon paracetamol exposure both at Day 7 and 20, and these changes in EP300 levels may change the number of active enhancers in the paracetamol exposed cells. Furthermore, we identified TFs such as EMX2, TBR1 and OTX2 whose regulatory activity is affected by paracetamol exposure at the differentiation end point. This is suggestive of a mechanism for how paracetamol exposure may change gene expression programmes in early brain development. More work is needed to follow up the functional role of paracetamol exposure on the enhancer regulation and gene expression.

We found a general dose-dependent increase in DNAm in paracetamol exposed cells compared to controls at both Day 7 and Day 20. The genes were enriched for BPs involved in cell morphogenesis and adhesion, but also synaptic transmission and signalling with a focus on catecholamines and GABAergic transmission. Considering that this is an in vitro system, the findings are compelling since structural cortical changes and catecholaminergic transmission have been the target of various epidemiological studies and drug clinical trials, both in children and adults with ADHD[77–80]. It is biologically plausible that medications that cross the placenta and the blood-brain barrier, may interfere with normal fetal brain neurodevelopment, previously shown for valproic acid, and more recently for topiramate[81]. This is especially relevant for substances that cross the blood-brain barrier, which is considered functional by the 8th week of gestation[82]. However, invasive testing of the fetal compartment in human is rarely indicated, which makes data on safety during pregnancy for most substances scant. Thus, most pharmacoepigenetic studies address associations of DNAm differences in cord blood or placenta from neonates delivered at term exposed to the maternal medication during pregnancy, which is also the case for paracetamol[83–85].

We previously found differentially methylated genes in cord blood from children with ADHD exposed to long-term maternal paracetamol use[20]. However, the causality, and relevance of such findings to brain development are not known. The hESCs used in our experiments represent the inner cell mass (ICM) of Day 6 preimplantation-blastocysts[86]. The ICM is known to differentiate to form the primitive ectoderm around Day 7.5 post fertilization[87], but placental circulation is not established before Day 17-20[88]. Prior to this, the fraction of paracetamol that reaches the developing embryo does so via passive diffusion[89]. Interestingly, irrespective of the temporal differences of the two models[90], comparing the differentially expressed and methylated genes identified in our study revealed overlap of several genes identified in cord blood with potential compelling relevance to early brain development. Notably, identification of a dose-specific effect on several genes have previously been shown to be associated with neural injury and toxic-insult response[91–93]. To our knowledge this is the first study that has identified an effect of paracetamol on differential DNAm of *KCNE3* in a neuronal differentiation model of hESCs. Differential DNAm at *KCNE3* was also identified in our MoBa study in cord blood[94]. Furthermore, *KCNE3* was also identified in a DNAm analysis of extremely low gestational age new born (ELGAN) cohort[83]. *KCNE3* is an interesting candidate, which encodes a voltage-gated ion channel with important functions in regulating release of neurotransmitters and neuronal excitability[95,96]. Among the overlapping genes, there was also *IER3*, whose differential DNA methylation at specific CpG sites has been previously associated with in utero exposure to bisphenol A (BPA)[97]. The same study had identified *TSPAN15*, which is also significantly differentially methylated between control and P200 cells in our neuronal differentiation model.

We also compared our data to previously published studies using the webtool (**hescneuroparacet**). In a rat model of fetal paracetamol exposure[98], dysregulation in specific ABC efflux transporters and related enzymes was found after chronic treatment of the mothers in E19 fetal brain and choroid plexus. In our model of paracetamol exposure, we also identified differential expression of the relevant genes *ABCA1, ABCC5, ABCD3* and *GSTM*3. Moreover, the expression of *ABCC4*, which encodes the multidrug resistance-associated protein MPRP4, known to play a role in paracetamol efflux was also upregulated at Day 20[99]. In another model assessing chronic paracetamol exposure effects in E15-19 rat brains[100], similar to our findings,

an increased expression of genes related to proliferation (e.g. *MKI67*, *MTDH*), cytoskeletal structural genes (e.g. *NEFL* at Day 20), metabolic stress alleviation (e.g. *PFKP* at Day 7) or decrease in genes related to differentiation (*SOX12* at Day 7) migration and dendrite orientation (such as *CRMP1* at Day 20) was found. Notably, a significant increase in *APOE* expression at P200 cells at Day 7 was observed indicating stress or neuronal damage[101], and a similar response by the increased expression for glutamate transporter *EAAT4*[102]. The significant *IL6ST* (GP130) and *MEF2A* [103] upregulation and the similarities of our findings to the other in vivo models, validate both the trajectories identified by our approach, and the chosen paracetamol neurotoxicity platform for early development studies.

Abiding by the Findability, Accessibility, Interoperability, and Reusability (FAIR) principles, we provide full access to the scRNA-seq and scATAC-seq datasets in open access shiny web platforms for scRNA-seq (**hescneuroparacet**) and integrative scATAC-seq/scRNA-seq (**hescneurodiffparacet**)[104,105]. These webtools allow for data correlation with other published gene expression datasets, and enable plotting, exporting, and downloading high resolution figures of gene expression and gene co-expression analysis UMAPs of any gene. Furthermore, there are multiple options for dataset exploration and visualization, such as heatmaps, violin-, box-, proportion- and bubble plots in different tabs, where gene expression may be viewed per cell, cluster, treatment and timepoint. Chromatin opening can be explored for genomic loci of interest for input sample, ATAC clusters or integrated clusters in a genome browser view with peak-to-gene link annotations (instantly plotted for 500 random cells each time). In addition, the processed datasets and code are made available for customization and integration with other studies. To our knowledge this is the first in vitro study of paracetamol exposure of hESCs under neuronal differentiation, that provides access to scRNA-seq and scATAC-seq data via interactive webtools.

Our study has several limitations and strengths. Protein expression changes were not explored, as this was beyond the scope of this study. This study aimed to delineate the epigenetic impact of paracetamol on early human cortical developmental events. We used both bulk- and scRNA- seq and comparing these two datasets identified a varying degree of overlapping DEGs from 1-27 %, confirming that both datasets are complementary to detect transcriptomic changes induced by paracetamol. Using a

multi-omics approach, we unveiled the diversified transcriptional networks related to paracetamol exposure. We could not accurately classify the maturation properties of the cells, or the proportion of cells in G0 phase, highlighting the necessity of new tools to deconvolute the neuronal G0 phase. The results of scATAC-seq analysis presented here are inherently limited by the relatively low genome-per-cell coverage. That means that some open chromatin regions that could have proved relevant for the individual cells or cell populations, may have been missed. Finally, the in vitro results presented here need to be validated by in vivo models and targeted human dataset exploration in future studies. This could confirm whether the pathways identified can explain the paracetamol-induced adverse effects in the early human brain.

Using an in vitro hESC model of neuronal development, we identified altered gene expression, DNAm and chromatin openness involved in key neuronal differentiation processes at bulk and single-cell RNA levels. An overlap of genes identified in this model and in the cord blood of neonates exposed long-term to paracetamol during pregnancy, points towards altered epigenetic regulation of early brain development. Identification of common DNAm modification sites and chromatin openness regions with a regulatory role on gene expression can identify loci and underlying mechanisms involved in neurotoxicity of drugs on the developing fetus with potential effect on long-term outcomes. Such findings could strengthen causal inference and clinical translation of altered DNAm, such as in cord blood, on brain development. However, these in vitro results need further validation for potential clinical translation.

Supplemental information

Supplemental Information includes seven figures and four tables.

Acknowledgements

We thank Knut Waagan (University of Oslo) for technical assistance. The majority of informatic analysis was performed at Saga super computing resources (Project NN9632K) provided by UNINETT Sigma2—the National Infrastructure for High Performance Computing and Data Storage in Norway. The sequencing service was provided by the Norwegian Sequencing Centre (www.sequencing.uio.no), a national technology platform hosted by Oslo University Hospital and the University of Oslo and

supported by the “Infrastructure” programs of the Research Council of Norway and the Southeastern Regional Health Authorities. PharmaTox Strategic Research Initiative was supported by Faculty of Mathematics and Natural Sciences, University of Oslo. We thank the Norwegian Centre for Stem Cell Research for discussions at the initiation of this project. We would also like to thank Akshay Akshay (University of Bern) for his help and fruitful discussion on single-cell ATAC-seq data analysis and visualization. We acknowledge funding from Research Council of Norway 262484 (R.E.), 241117 (R.L.), and 287953 (A.S.); the Swedish Research Council 2019-01157 (A.S.) and grants from the Swedish Brain FO2019-0087 (A.S.) and the Freemasons Children's House of Stockholm (A.S.) and BiomatDB+ (Horizon Europe #101058779; AS). We thank University of Oslo for open access publication support. The funders played no role in study design, data collection, data analyses, interpretation, or writing of the article. The graphical abstract was generated in Biorender.com.

Author Contributions

Conceptualization, M.S., A.S., R.E., K.G. and R.L.; Methodology, A.S., M.S., R.L., S.M., K.G., R.E., A.Sh., M.L., and M.F.; Writing – Original Draft, A.S., M.S., A.Sh., R.E., K.G. and R.L.; Writing – Review & Editing, A.S., M.S. R.L., K.G., R.E., A.Sh., M.L., H.N., and G.A.; Software, Formal Analysis, and Visualization, M.S., A.Sh., K.G., A.Y.M.S., R.L., and R.E.; Investigation and Validation, A.S., M.S., M.L., M.F., S.M., R.E. and K.G.; Funding, R.L., K.G., A.S., and R.E.; Supervision, R.L., K.G., H.N., A.S., and R.E.; Resources G.A., R.L., and R.E. All authors read and approved the final manuscript.

Declaration of Interest

The authors declare no competing interest.

Authors' information

Ankush Sharma is now an employee of Acerta-Pharma, The Netherlands.

STAR Methods

REAGENT or RESOURCE	SOURCE	IDENTIFIER
Antibodies		
N/A	N/A	N/A
Chemicals, peptides, and recombinant proteins		
Geltrex™ LDEV-Free, hESC-Qualified, Reduced Growth Factor Basement Membrane Matrix	ThermoFisher	A1413302
KnockOut™ DMEM	ThermoFisher	10829018
PBS, no calcium, no magnesium	ThermoFisher / GIBCO	14190
Dimethyl-sulfoxide, DMSO	Sigma-Aldrich/ Merck	D8418
Accutase™ Cell Detachment Solution	STEMCELL Technologies	7920
UltraPure 0.5 M EDTA, pH 8.0	ThermoFisher	15575020
Paracetamol	Sigma-Aldrich/Merck	A7085
RHO/ROCK Pathway Inhibitor Y-27632	STEMCELL Technologies	SCM075
Essential 8™ Medium	ThermoFisher	A1517001
Poly-L-ornithine hydrobromide	Sigma-Aldrich/ Merck	P3655
Fibronectin (Bovine Protein, Plasma)	ThermoFisher	33010018
N2 supplement (100X)	ThermoFisher	17502048
Advanced DMEM/F-12	ThermoFisher	12634028
GlutaMAX™ Supplement	GIBCO/ ThermoFisher	35050061
Penicillin Streptomycin (10,000 U/mL)	ThermoFisher	15140122
LDN-193189	STEMCELL Technologies	72148
SB 431542 (hydrate)	Sigma-Aldrich / Merck	S4317
XAV939	STEMCELL Technologies	72674
B-27™ Supplement (50X), serum free	ThermoFisher	17504044
Recombinant Human FGF basic	Peprotech	100-18B
Recombinant Human EGF, Animal-Free	Peprotech	AF-100-15
Critical commercial assays		
Countess™ Cell Counting Chamber Slides	ThermoFisher	C10312
RNeasy Mini Kit	Qiagen	74106
RNAse-Free DNase Set	Qiagen	79254
RNA/DNA purification kit	Norgen Biotek Corp.	298-48700
RNase-Free DNase I Kit	Norgen Biotek Corp.	298-25720
Qubit™ RNA BR Assay Kit	ThermoFisher/Invitrogen	Q10211
QuantiTect Reverse Transcription Kit	Qiagen	205311
ddPCR Supermix for Probes (no dUTP)	BioRad	186-3024
Droplet Generation Oil for Probes	BioRad	186-3005
TruSeq Stranded mRNA Library Prep Kit	Illumina	20020595
IDT for Illumina – TruSeq RNA UD Indexes	Illumina	20022371
NovaSeq 6000 S1 Reagent Kit v1.5 (200 cycles)	Illumina	20028318
Infinium MethylationEPIC BeadChip Kit (96 samples)	Illumina	WG-317-1003
30 mm MACS SmartStrainers	Miltenyi Biotech	130-110-915
Chromium Single Cell 3´ Library & Gel Bead Kit v3	10x Genomics	1000075

Chromium i7 Multiplex Kit	10x Genomics	120262
NextSeq 500/550 High Output Kit (150 Cycles)	Illumina	20024907
Next GEM Chip H Single Cell Kit	10x Genomics	1000162
Next GEM Single Cell ATAC Library & Gel Bead Kit v1.1	10x Genomics	1000176
Chromium i7 Multiplex Kit N Set A	10x Genomics	1000084
NovaSeq 6000 SP Reagent Kit (100 cycles)	Illumina	20028401
Deposited data		
RNA-seq, DNAm, Infinium Methylation EPIC, scRNA-seq & scATAC-seq	This paper	NCBI GEO: GSE220027 (Subseries GSE220023, GSE220024, GSE220025, GSE220026)
RNA-seq, DNAm, Infinium Methylation EPIC, scRNA-seq & scATAC-seq	(Samara et al., 2022)[106]	NCBI GEO: GSE192858 (Subseries GSE192854, GSE192855, GSE192856, GSE192857)
Experimental models: Cell lines		
Human embryonic cells, HS360, 46XY	Stockholms Medicinska Biobank / Sweden	HS360
Oligonucleotides		
POU5F1	ThermoFisher/TaqMan™	Hs00999632_g1
SOX2	ThermoFisher/TaqMan™	Hs01053049_s1
NANOG	ThermoFisher/TaqMan™	Hs04399610_g1
NES	ThermoFisher/TaqMan™	Hs04187831_g1
FOXG1	ThermoFisher/TaqMan™	Hs01850784_s1
TUBB3	ThermoFisher/TaqMan™	Hs00801390_s1
MAP2	ThermoFisher/TaqMan™	Hs00258900_m1
PAX6	ThermoFisher/TaqMan™	Hs00240871_m1
OTX2	ThermoFisher/TaqMan™	Hs00222238_m1
VIM	ThermoFisher/TaqMan™	Hs00958111_m1
NEUROD1	ThermoFisher/TaqMan™	Hs01922995_s1
RPL30	ThermoFisher/TaqMan™	Hs00265497_m1
RAF1 F: tgggaaatagaagccagtgaa R: cctttaggatctttactgcaacatc	Eurofins	Probe 56 4688538001
Software and algorithms		
R Programming language	(R Core Team, 2019)[107]	https://www.r-project.org/

ArchR1.0.1	(Granja et al., 2021)[53]	https://www.archrproject.com
Seurat Version 4	(Hao et al., 2021; Stuart et al., 2019)[108,109]	https://github.com/satijalab/seurat
Signac	(Stuart et al., 2021)[110]	https://satijalab.org/signac/
BSgenome1.58.0	(Pages, 2020)[111]	https://rdrr.io/bioc/BSgenome/
ShinyCell	(Ouyang et al., 2021)[112]	https://github.com/SGDDNB/ShinyCell
ShinyArchR.UiO	(Sharma et al., 2021)[113]	https://github.com/EskelandLab/ShinyArchRUiO
CytoTRACE R package (v0.3.3)	(Gulati et al., 2020)[114]	https://cytotrace.stanford.edu
10x Genomics Cell Ranger -Count and 10x Genomics Cell Ranger -Count ATAC	10x genomics	https://www.10xgenomics.com
BSgenome.Hsapiens.UCSC.hg38	DOI:10.18129/B9.bioc.BSgenome.Hsapiens.UCSC.hg38 (The Bioconductor Dev Team, 2021) [115]	https://bioconductor.org/packages/release/data/annotation/html/BSgenome.Hsapiens.UCSC.hg38.html
EnsDb.Hsapiens.v86	DOI:10.18129/B9.bioc.EnsDb.Hsapiens.v86 (Rainer, 2017) [116]	https://bioconductor.org/packages/release/data/annotation/html/EnsDb.Hsapiens.v86.html
clustree	(Zappia and Oshlack, 2018)[117]	https://cran.r-project.org/web/packages/clustree/vignettes/clustree.html#references
scater	(McCarthy et al., 2017)[118]	https://bioconductor.org/packages/release/bioc/html/scater.html
DEseq2	(Love et al., 2014)[119]	https://bioconductor.org/packages/release/bioc/html/DESeq2.html
GSEA	(Subramanian et al., 2005)[120]	https://www.gsea-msigdb.org/gsea/index.jsp
Minfi	(Aryee et al., 2014)[121]	https://www.bioconductor.org/packages/release/bioc/html/minfi.html
Limma	(Ritchie et al., 2015)[122]	https://bioconductor.org/packages/release/bioc/html/limma.html
methylGSA	(Ren and Kuan et al., 2019)[123]	https://bioconductor.org/packages/release/bioc/html/methylGSA.html
SingleR	(Aran et al., 2019)[124]	https://github.com/dviraran/SingleR

Harmony	(Korsunsky et al., 2019)[125]	https://github.com/immunogenomics/harmony
GREAT	(McLean et al., 2010)[126]	http://great.stanford.edu/public/html/
Intervene	(Khan and Mathelier, 2017)[127]	https://github.com/asntech/intervene-shiny
gprofiler	(Kolberg et al., 2020)[128]	https://biit.cs.ut.ee/gprofiler/gost
MACS2	(Feng et al., 2012)[129]	https://pypi.org/project/MACS2/ https://github.com/macs3-project/MACS
refdata-cellranger-atac-hg38-version refdata-	10x genomics	https://support.10xgenomics.com/single-cell-atac/software/downloads/
JASPAR	(Bryne et al., 2008)[130]	https://bioconductor.org/packages/release/data/annotation/html/JASPAR2020.html http://jaspar.genereg.net
Single Cell Experiment	(Amezquita et al., 2020)[131]	https://bioconductor.org/packages/release/bioc/html/SingleCellExperiment.html
Escape	DOI:10.18129/B9.bioc.escape; [132]	https://github.com/ncborcherding/escape
ggseqlogo	Omar Wagih, 2017	https://CRAN.R-project.org/package=ggseqlogo
TFBSTools	10.18129/B9.bioc.TFBSTools	https://bioconductor.org/packages/release/bioc/html/TFBSTools.html
uwot	James Melville, 2022	https://CRAN.R-project.org/package=uwot
viridisLite	(Garnier et al., 2021)[133]	https://cran.r-project.org/web/packages/viridisLite/index.html
ShinyGO	(Ge et al., 2020)[134]	http://bioinformatics.sdstate.edu/go/
Python3	(Van Rossum and Drake, 2009)[135]	https://www.python.org/downloads/
10x Genomics Loupe Browser	10x genomics	https://www.10xgenomics.com
ComplexHeatmap	(Gu, 2022; Gu et al., 2016)[136,137]	https://jokergoo.github.io/ComplexHeatmap-reference/book/

ggplot2	(Wickham, 2009)[138]	https://cran.r-project.org/web/packages/ggplot2/index.html
igraph	igraph	https://igraph.org
IRanges	(Lawrence et al., 2013)[139]	https://bioconductor.org/packages/release/bioc/html/IRanges.html
Reticulate	Tomasz Kalinowski, R Studio	https://CRAN.R-project.org/package=reticulate
tidyverse	(Wickham et al., 2019)[140]	https://www.tidyverse.org/packages/
ggpubr	(Kassambara, 2020)[141]	https://cran.r-project.org/web/packages/ggpubr/index.html
SARTools	(Varet et al., 2016)[142]	https://github.com/PF2-pasteur-fr/SARTools
pheatmap	Raivo Kolde, 2019	https://CRAN.R-project.org/package=pheatmap
IlluminaHumanMethylationEPICmanifest	Kasper Daniel Hansen, 2016	https://bioconductor.org/packages/release/data/annotation/html/IlluminaHumanMethylationEPICmanifest.html
IlluminaHumanMethylationEPICanno.ilm10b5.hg38	EPIC annotation 1.0 B5	https://github.com/achilleasNP/IlluminaHumanMethylationEPICanno.ilm10b5.hg38
Rstudio	RStudio Team	https://www.rstudio.com/

Shiny single-cell tools for visualisation of datasets.	This paper	Custom scripts for computational analysis are available at https://github.com/EskelandLab/Neuralparacet. The single-cell data can be explored in webtools for scRNA-seq (**hescneuroparacet**) and integrative scATAC-seq/scRNA-seq (**hescneurodiffparacet**) at https://cancell.medisin.uio.no/.

RESOURCE AVAILABILITY

Lead contact

Further information and requests for resources and reagents should be directed to and will be fulfilled by the lead contact Ragnhild Eskeland (Ragnhild.Eskeland@medisin.uio.no).

Materials availability

This study did not generate new unique reagents.

Data and code availability

- All original code can be found at https://github.com/EskelandLab/Neuralparacet. DOIs are listed in the key resources table.
- The single-cell RNA-seq/ATAC-seq, RNA-seq and DNA-methylation data reported in this study cannot be deposited in a public repository because the data could be potentially traced back to a single embryo and the donor. To request access, contact the lead author and the Stockholm Medical Biobank. It may be required to establish a Personal Data processing (PDP) Agreement and/or Data Transfer Agreement (DTA) according to General Data Protection Regulation (GDPR).

- Processed datasets have been deposited at NCBI's GEO. Accession numbers are listed in the key resources table. Single-cell data are shared for visualization in two open access webtools at https://cancell.medisin.uio.no: (**hescneuroparacet**) https://cancell.medisin.uio.no/scrna/hescneuroparacet/ and (**hescneurodiffparacet**) https://cancell.medisin.uio.no/scatac/hescneurodiffparacet/

EXPERIMENTAL MODEL AND SUBJECT DETAILS

hESC culture and maintenance

hESCs HS360 (Karolinska Institutet, Sweden, RRID:CVCL C202)[86,143] were cultured as described by Samara et al, 2022[24]. In brief, cells were maintained in Essential 8™ Medium, on Geltrex pre-coated culture plates. Cells were routinely passaged at 75-85% confluency using 0.5 mM ethylenediaminetetraacetic acid (EDTA) in ratios between 1:3 to 1:6. When hESCs were collected for initiation of the differentiation protocol and Accutase was used to detach and dissociate cells.

Neuronal differentiation of hESCs and exposure to paracetamol

hESCs HS360 were differentiated, as described[24], in two separate time-course experiments, to investigate the in vitro effects of paracetamol exposure in physiologically concentrations relevant to long-term exposure in vivo. Since paracetamol crosses the placenta and the blood-brain barrier and has an insignificant plasma protein binding, maternal plasma/serum and cord blood concentrations can be used as estimates for the amount of paracetamol that reaches the developing fetal brain[144–147]. Concentrations of 100 µM and 200 µM paracetamol were chosen as range for physiological plasma peak concentration in vivo, corresponding to one intermediate and one high peak plasma concentration[25–27]. Thus, cells undergoing neuronal differentiation were exposed to changes of medium only (control) or medium containing 100 or 200 µM paracetamol from Day 1 to Day 20. Control cells were harvested at day 0, 7, 13 and 20, while cells exposed to 100 or 200 µM paracetamol were harvested at Day 7 and 20.

METHODS DETAILS

DNA/RNA isolation

Genomic DNA and total RNA were isolated by direct lysis in the culture vessels followed by column-based isolation using RNA/DNA purification kit (Norgen Biotek). RNase-Free DNase I Kit (Norgen Biotek) was applied for on-column removal of genomic DNA contamination from RNA isolates. Five RNA isolates were processed using the RNeasy Mini Kit (Qiagen) followed by DNase-treatment using the RNAse-Free DNase Set (Qiagen). All isolations were performed according to the manufacturer's instructions. Nucleic acid quantification was performed using Qubit (ThermoFisher Scientific), purity was measured using Nanodrop 2000 (ThermoFisher Scientific), while RNA and DNA integrity was assessed using 2100 Bioanalyzer (Agilent Technologies) and 4200 TapeStation (Agilent Technologies), respectively.

ddPCR and RNA expression analysis

Reverse transcription of total RNA was performed using QuantiTect Reverse Transcription Kit (Qiagen). Subsequent ddPCR reactions were set up using ddPCR Supermix for Probes (No dUTP) (BioRad) and Taqman assays (ThermoFisher) or Universal Probes (Roche) in combination with target primers (Eurofins) as outlined in key resources table. Droplets for ddPCR amplification were generated using the QX200 Droplet Generator (BioRad). Data acquisition and primary analysis was done using the QX200 Droplet Reader (BioRad) and QuantaSoft software (BioRad). All steps were performed according to the manufacturer's instructions. To calculate the number of target copies per ng RNA input, samples were normalized using RPL30 and RAF1 as normalization genes[148]. Statistical comparisons were performed in R using t-test in ggpubr package v.0.4.0[141]. Results were visualized in R using the tidyverse package[140].

Bulk RNA-seq

The sequencing library was prepared with TruSeq Stranded mRNA Library Prep (Illumina) according to manufacturer's instructions. The libraries (n=39) were pooled at equimolar concentrations and sequenced on an Illumina NovaSeq 6000 S1 flow cell (Illumina) with 100 bp paired end reads. The quality of sequencing reads was assessed using BBMap v.34.56[149] and adapter sequences and low-quality reads were

removed. The sequencing reads were then mapped to the GRCh38.p5 index (release 83) using HISAT2 v.2.1.0[150]. Mapped paired end reads were counted to protein coding genes using featureCounts v.1.4.6-p1[151]. Differential expression analysis was conducted in R version 3.5.1[152] using SARTools v.1.6.8[142] and the DESeq2 v.1.22.1 [153], and genes were considered significantly differentially expressed with an FDR < 0.05. Normalized counts were visualized using the tidyverse package v.1.3.[140]. The heatmaps were generated using the pheatmap package version 1.0.12[154]. The Wald-test was used to calculate p-values and Benjamini-Hochberg was used to correct for multiple testing. The GSEA analysis of ranked lists of differentially expressed genes were performed using GSEA software v.4.1.0[120] to identify enrichment of BP terms.

Bulk DNAm analysis

DNAm status of 43 samples were assessed using the Infinium MethylationEPIC BeadChip v.1.0_B3 (Illumina). Quality control and pre-processing of the raw data was performed in R using Minfi v.1.36.0[121]. No samples were removed due to poor quality (detection p values >0.05). Background correction was performed using NOOB method [155] and β values (ratio of methylated signal divided by the sum of the methylated and unmethylated signal) were normalized using functional normalization [156]. Probes with unreliable measurements (detection p values >0.01) (n = 12,538) and cross-reactive probes (45) (n = 42,844) were then removed, resulting in a final dataset consisting of 810,477 probes and 43 samples. Probes were annotated with Illumina Human Methylation EPIC annotation 1.0 B5 (hg38). Differential DNAm analysis was performed on the M values (log2 of the β values) using the limma package[122], and CpGs were considered significantly differentially methylated with an FDR < 0.05. GO analysis of BP terms was performed using p-values of increasing or decreasing CpGs (DMCs) as input to methylRRA function implemented in the methylGSA package version 1.14.0[123].

Collection of cells and scRNA-seq

Cells were washed twice in wells with 1x PBS and detached using Accutase (STEMCELL Technologies) at 37 °C for 7 min. Cells were triturated 10-15 times to separate into single cells and transferred to centrifuge tubes containing the appropriate base media with 0.05 % BSA (Sigma-Aldrich). Counts were performed using Countess II FL Cell Counter (ThermoFisher Scientific) before cells were centrifuged at 300x g

for 5 min and the supernatant was discarded. Cell pellets were then resuspended in base medium containing 0.05 % BSA and cell aggregates were filtered out using MACS SmartStrainers (Miltenyi). The cells were recounted and processed within 1 hour on the 10x Chromium controller (10x Genomics). Approximately 2,300 cells were loaded per channel on the Chromium Chip B (10x Genomics) to give an estimated recovery of 1,400 cells. The Chromium Single Cell 3´ Library & Gel Bead Kit v3 (10x Genomics) and Chromium i7 Multiplex Kit (10x Genomics) were used to generate scRNA-seq libraries, according to the manufacturer's instructions. Libraries from 16 samples were pooled together based on molarity and sequenced on a NextSeq 550 (Illumina) with 28 cycles for read 1, 8 cycles for the I7 index and 91 cycles for read 2. For the second sequencing run, libraries were pooled again based on the number of recovered cells to give a similar number of reads per cell for each sample (33,000 - 44,000 reads/cell).

scRNA-seq data analysis

The Cell Ranger 3.1.0 Gene Expression pipeline (10x Genomics) was used to demultiplex the raw base-call files and convert them into FASTQ files. The FASTQ files were aligned to the GRCh38 human reference genome, and the Cell Ranger Count command quantified single-cell read counts using default parameters for Days 7 and 20. Cell ranger aggregate was used for aggregating counts of replicates. The Seurat Package v.4.1.0[109] was used to perform quality control and normalization on the count matrices. We filtered cells with number of RNA counts >= 2000 & <= 50000 to remove dead cells, doublets and multiplets. The cells expressing fewer genes (less than 200) and genes expressed in less than 3 cells were excluded from the downstream analysis. Outlier cells with high Mitochondrial percentage was computed using Scater package 1.0.4 “isoutlier” function with nmads parameter of 5[118]. Counts were adjusted for cell-specific sampling using the SCTransform function with regression of Cell cycle genes and Mitochondrial content[157,158].

We used a resolution of 0.4 to cluster cells, obtained by determining the optimum number of clusters (cells grouped together sharing similar expression profiles) in the dataset using the Clustree R package[117]. Principal component analysis was performed using the RunPCA function, followed by FindClusters and RunUMAP functions of Seurat package to perform SNN-based UMAP clustering.

FindMarkers from the Seurat R package were used to perform differential expression analysis between groups. For DE between exposure groups, thresholds were set to the following: min.pct = 0.25, min.diff.pct = -Inf, logfc.threshold = 0.1. For top overlapping DE genes per Day (Fig. 6 E/J), thresholds were set to the following: min.pct = 0.25, min.diff.pct = -Inf, logfc.threshold = 0.25. Genes with an adjusted p-value < 0.05 were considered significant. GO analysis was performed using the DEenrichRPlot function of the mixscape R package with the "GO_Biological_Process_2018" database with the following thresholds: logfc.threshold = 0.25, max genes = 500. The SingleR R package [124] was used to annotate the cells against reference data sets from a Human Brain dataset [46] from the scRNAseq R package [159]. Cell types with < 15 cells annotated were excluded from the plots.

scATAC-seq Library preparation and sequencing

Cells were washed twice with 1xPBS and detached to single cell suspension by application of Accutase (STEMCELL Technologies) at 37 °C for 7 min. The detached cells were washed with appropriate base media with added 0.04% BSA (Sigma-Aldrich) and filtered using MACS SmartStrainers (Miltenyi Biotech) to remove cell aggregates. Nuclei isolation was done according to the 10x Genomics protocol CG000169 (Rev D) using 2 minutes of incubation in a lysis buffer diluted to 0.1x and 0.5x for Day 0 and Day 20 cells, respectively. Countess II FL Cell Counter (ThermoFisher Scientific) was used to quantify nuclei and confirm complete lysis and microscopy to confirm high nuclei quality. Nuclei were further processed on the 10x Chromium controller (10x Genomics) using Next GEM Chip H Single Cell Kit (10x Genomics), Next GEM Single Cell ATAC Library & Gel Bead Kit v1.1 (10 x Genomics) and Chromium i7 Multiplex Kit N Set A (10x Genomics) according to the Next GEM Single Cell ATAC Reagent Kits v1.1 User Guide (CG000209, Rev C). The targeted nuclei recovery was 5,000 nuclei per sample. The resulting 4 sample libraries were sequenced on a NovaSeq Sp flow cell (Illumina) with 50 cycles for read 1, 8 cycles for the i7 index read, 16 cycles for the i5 index read and 49 cycles for read 2.

scATAC sequencing analysis

Cell Ranger ATAC version 1.2.0 with reference genome GRCh38-1.2.0 was used to pre-process scATAC-seq raw sequencing data into FASTQ files. Single-cell accessibility counts for the cells were generated from reads using the *cellranger-atac count* pipeline. Reference genome HG38 used for alignment and generation of single-cell accessibility counts was obtained from the 10x Genomics (https://support.10xgenomics.com/single-cell-atac/software/downloads/).

Downstream analysis of the scATAC-seq data was performed using the R package ArchR v1.0.1[53]. A tile matrix of 500-bp bins was constructed after quality control, removal of low-quality cells and doublet removal using the doubletfinder function of ArchR. The ArchR Project contained the filtered cells that had a TSS enrichment below 3 and <1000 fragments. A layered dimensionality reduction approach utilizing Latent Semantic Indexing (LSI) and Singular Value Decomposition (SVD) applied on Genome-wide tile matrix. Uniform Manifold approximation and projection (UMAP) was performed to visualize data in 2D space. Louvain Clustering methods implemented in R package Seurat[109] were used for clustering of the single-cell accessibility profiles.

QUANTIFICATION AND STATISTICAL ANALYSIS

Statistical analyses were performed in R version 4.1.2[107] applying SARTools v.1.6.8[142], DESeq2 v.1.22.1[119], Limma[122], ArchR[53], Seurat[108,109], and ggpubr package v.0.4.0 [141]. Details are described in the relevant methods sections above.

References

1. Lupattelli, A., Spigset, O., Twigg, M.J., Zagorodnikova, K., Mårdby, A.C., Moretti, M.E., Drozd, M., Panchaud, A., Hämeen-Anttila, K., Rieutord, A., et al. (2014). Medication use in pregnancy: A cross-sectional, multinational web-based study. BMJ Open *4*, 4365. 10.1136/bmjopen-2013-004365.

2. Zablotsky, B., Black, L.I., Maenner, M.J., Schieve, L.A., Danielson, M.L., Bitsko, R.H., Blumberg, S.J., Kogan, M.D., and Boyle, C.A. (2019). Prevalence and Trends of Developmental Disabilities among Children in the United States: 2009–2017. Pediatrics *144*, e20190811. 10.1542/peds.2019-0811.

3. Nordeng, H., Ystrøm, E., and Einarson, A. (2010). Perception of risk regarding the use of medications and other exposures during pregnancy. European Journal of Clinical Pharmacology *66*, 207–214. 10.1007/s00228-009-0744-2.

4. Werler, M.M., Mitchell, A.A., Hernandez-Diaz, S., and Honein, M.A. (2005). Use of over-the-counter medications during pregnancy. American Journal of Obstetrics and Gynecology *193*, 771–777. 10.1016/j.ajog.2005.02.100.

5. Mcelhatton, P.R., Sullivan, F.M., and Volans, G.N. (1997). Paracetamol overdose in pregnancy analysis of the outcomes of 300 cases referred to the Teratology Information Service. Reproductive Toxicology, 85–94. 10.1016/S0890-6238(96)00200-6.

6. Liew, Z., Ritz, B., Rebordosa, C., Lee, P.-C., and Olsen, J. (2014). Acetaminophen Use During Pregnancy, Behavioral Problems, and Hyperkinetic Disorders. JAMA Pediatrics *168*, 313. 10.1001/jamapediatrics.2013.4914.

7. Brandlistuen, R.E., Ystrom, E., Nulman, I., Koren, G., and Nordeng, H. (2013). Prenatal paracetamol exposure and child neurodevelopment: a sibling-controlled cohort study. International Journal of Epidemiology *42*, 1702–1713. 10.1093/ije/dyt183.

8. Avella-Garcia, C.B., Julvez, J., Fortuny, J., Rebordosa, C., García-Esteban, R., Galán, I.R., Tardón, A., Rodríguez-Bernal, C.L., Iñiguez, C., Andiarena, A., et al. (2016). Acetaminophen use in pregnancy and neurodevelopment: attention function and autism spectrum symptoms. International Journal of Epidemiology *45*, dyw115. 10.1093/ije/dyw115.

9. Stergiakouli, E., Thapar, A., and Davey Smith, G. (2016). Association of Acetaminophen Use During Pregnancy With Behavioral Problems in Childhood. JAMA Pediatrics *170*, 964. 10.1001/jamapediatrics.2016.1775.

10. Thompson, J.M.D., Waldie, K.E., Wall, C.R., Murphy, R., Mitchell, E.A., and ABC study group (2014). Associations between Acetaminophen Use during Pregnancy and ADHD Symptoms Measured at Ages 7 and 11 Years. PLoS ONE *9*, e108210. 10.1371/journal.pone.0108210.

11. Bornehag, C.-G., Reichenberg, A., Hallerback, M.U., Wikstrom, S., Koch, H.M., Jonsson, B.A., and Swan, S.H. (2018). Prenatal exposure to acetaminophen and children's language development at 30 months. European psychiatry : the journal of the Association of European Psychiatrists *51*, 98–103. 10.1016/j.eurpsy.2017.10.007.

12. Ystrom, E., Gustavson, K., Brandlistuen, R.E., Knudsen, G.P., Magnus, P., Susser, E., Smith, G.D., Stoltenberg, C., Surén, P., Haberg, S.E., et al. (2017). Prenatal exposure to acetaminophen and risk of ADHD. Pediatrics *140*, 20163840. 10.1542/peds.2016-3840.

13. Trønnes, J.N., Wood, M., Lupattelli, A., Ystrom, E., and Nordeng, H. (2020). Prenatal paracetamol exposure and neurodevelopmental outcomes in preschool-aged children. Paediatric and Perinatal Epidemiology *34*, 247–256. 10.1111/ppe.12568.

14. Khan, F.Y., Kabiraj, G., Ahmed, M.A., Adam, M., Mannuru, S.P., Ramesh, V., Shahzad, A., Chaduvula, P., and Khan, S. (2022). A Systematic Review of the Link Between Autism Spectrum Disorder and Acetaminophen: A Mystery to Resolve. Cureus *14*. 10.7759/CUREUS.26995.

15. European Medicines Agency (EMA), and Pharmacovigilance Risk Assessment Committee (PRAC) (2019). PRAC recommendations on signals. https://www.ema.europa.eu/en/documents/prac-recommendation/prac-recommendations-signals-adopted-12-15-march-2019-prac-meeting_en.pdf.

16. Bauer, A.Z., Swan, S.H., Kriebel, D., Liew, Z., Taylor, H.S., Bornehag, C.G., Andrade, A.M., Olsen, J., Jensen, R.H., Mitchell, R.T., et al. (2021). Paracetamol use during pregnancy — a call for precautionary action. Nature Reviews Endocrinology 2021 17:12 *17*, 757–766. 10.1038/S41574-021-00553-7.

17. The European Network of Teratology Information Services (ENTIS) (2021). Position statement on acetaminophen (paracetamol) in pregnancy. https://www.entis-org.eu/wp-content/uploads/2021/10/ENTIS-position-statement-on-acetaminophen-3.10.2021.pdf.

18. Alwan, S., Conover, E.A., Harris-Sagaribay, L., Lamm, S.H., Lavigne, S.V., Lusskin, S.I., Obican, S.G., Romeo, A.N., Scialli, A.R., and Wisner, K.L. (2022). Paracetamol use in pregnancy — caution over causal inference from available data. Nat Rev Endocrinol *18*, 190–190. 10.1038/s41574-021-00606-x.

19. Damkier, P., Cleary, B., Weber-Schoendorfer, C., Shechtman, S., Cassina, M., Panchaud, A., and Diav-Cirtin, O. (2022). Handle with care — interpretation, synthesis and dissemination of data on paracetamol in pregnancy. Nat Rev Endocrinol *18*, 191–191. 10.1038/s41574-021-00605-y.

20. Gervin, K., Nordeng, H., Ystrom, E., Reichborn-Kjennerud, T., and Lyle, R. (2017). Long-term prenatal exposure to paracetamol is associated with DNA methylation differences in children diagnosed with ADHD. Clinical Epigenetics *9*, 77. 10.1186/s13148-017-0376-9.

21. Fragou, D., Pakkidi, E., Aschner, M., Samanidou, V., and Kovatsi, L. (2019). Smoking and DNA methylation: Correlation of methylation with smoking behavior and association with diseases and fetus development following prenatal exposure. 10.1016/j.fct.2019.04.059.

22. Cornelius, M.D., De Genna, N.M., Leech, S.L., Willford, J.A., Goldschmidt, L., and Day, N.L. (2011). Effects of prenatal cigarette smoke exposure on neurobehavioral outcomes in 10-year-old children of adolescent mothers. Neurotoxicology and Teratology *33*, 137–144. 10.1016/j.ntt.2010.08.006.

23. Tran, N.Q.V., and Miyake, K. (2017). Neurodevelopmental Disorders and Environmental Toxicants: Epigenetics as an Underlying Mechanism. International Journal of Genomics *2017*. 10.1155/2017/7526592.

24. Samara, A., Falck, M., Spildrejorde, M., Leithaug, M., Acharya, G., Lyle, R., and Eskeland, R. (2022). Robust neuronal differentiation of human embryonic stem cells for neurotoxicology. STAR Protocols *3*, 101533. 10.1016/j.xpro.2022.101533.

25. Graham, G.G., Davies, M.J., Day, R.O., Mohamudally, A., and Scott, K.F. (2013). The modern pharmacology of paracetamol: Therapeutic actions, mechanism of action, metabolism, toxicity and recent pharmacological findings. Inflammopharmacology *21*, 201–232. 10.1007/s10787-013-0172-x.

26. Trettin, A., Böhmer, A., Suchy, M.T., Probst, I., Staerk, U., Stichtenoth, D.O., Frölich, J.C., and Tsikas, D. (2014). Effects of paracetamol on NOS, COX, and CYP activity and on

oxidative stress in healthy male subjects, rat hepatocytes, and recombinant NOS. Oxidative Medicine and Cellular Longevity *2014*. 10.1155/2014/212576.

27. Raffa, R.B., Pawasauskas, J., Pergolizzi, J. V., Lu, L., Chen, Y., Wu, S., Jarrett, B., Fain, R., Hill, L., and Devarakonda, K. (2018). Pharmacokinetics of Oral and Intravenous Paracetamol (Acetaminophen) When Co-Administered with Intravenous Morphine in Healthy Adult Subjects. Clinical Drug Investigation *38*, 259–268. 10.1007/s40261-017-0610-4.

28. Samara, A., Spildrejorde, M., Sharma, A., Gervin, K., Lyle, R., and Eskeland, R. (2022). A multi-omics approach to visualize early neuronal differentiation from hESCs in 4D. iScience. 10.1016/j.isci.2022.105279.

29. Simões-Costa, M., and Bronner, M.E. (2015). Establishing neural crest identity: a gene regulatory recipe. Development (Cambridge, England) *142*, 242. 10.1242/DEV.105445.

30. Pensold, D., and Zimmer, G. (2018). Single-Cell Transcriptomics Reveals Regulators of Neuronal Migration and Maturation During Brain Development. Journal of Experimental Neuroscience *12*. 10.1177/1179069518760783.

31. Guo, H., Duyzend, M.H., Coe, B.P., Baker, C., Hoekzema, K., Gerdts, J., Turner, T.N., Zody, M.C., Beighley, J.S., Murali, S.C., et al. (2019). Genome sequencing identifies multiple deleterious variants in autism patients with more severe phenotypes. Genetics in medicine : official journal of the American College of Medical Genetics *21*, 1611. 10.1038/S41436-018-0380-2.

32. Chen, J., Yen, A., Florian, C.P., and Dougherty, J.D. (2022). MYT1L in the making: emerging insights on functions of a neurodevelopmental disorder gene. Translational Psychiatry *12*. 10.1038/S41398-022-02058-X.

33. Roesler, M.K., Lombino, F.L., Freitag, S., Schweizer, M., Hermans-Borgmeyer, I., Schwarz, J.R., Kneussel, M., and Wagner, W. (2019). Myosin XVI Regulates Actin Cytoskeleton Dynamics in Dendritic Spines of Purkinje Cells and Affects Presynaptic Organization. Frontiers in Cellular Neuroscience *13*. 10.3389/FNCEL.2019.00330/FULL.

34. Maïza, A., Sidahmed-Adrar, N., Michel, P.P., Carpentier, G., Habert, D., Dalle, C., Redouane, W., Hamza, M., van Kuppevelt, T., Ouidja, M.O., et al. (2020). 3-O-sulfated heparan sulfate interactors target synaptic adhesion molecules from neonatal mouse brain and inhibit neural activity and synaptogenesis in vitro. Scientific Reports *10*. 10.1038/S41598-020-76030-4.

35. Zhang, Y., Li, Y., Fan, Y., Zhang, X., Tang, Z., Qi, J., Zhao, B., Li, F., Chen, X., Liang, H., et al. (2022). SorCS3 promotes the internalization of p75NTR to inhibit GBM progression. Cell Death & Disease *13*. 10.1038/S41419-022-04753-5.

36. Tu, L., Fukuda, M., Tong, Q., and Xu, Y. (2022). The ventromedial hypothalamic nucleus: watchdog of whole-body glucose homeostasis. Cell & Bioscience *12*. 10.1186/S13578-022-00799-2.

37. Yap, C.C., Digilio, L., McMahon, L., and Winckler, B. (2017). The endosomal neuronal proteins Nsg1/NEEP21 and Nsg2/P19 are itinerant, not resident proteins of dendritic endosomes. Scientific Reports *7*. 10.1038/S41598-017-07667-X.

38. Tábara, L.C., Al-Salmi, F., Maroofian, R., Al-Futaisi, A.M., Al-Murshedi, F., Kennedy, J., Day, J.O., Courtin, T., Al-Khayat, A., Galedari, H., et al. (2022). TMEM63C mutations cause mitochondrial morphology defects and underliehereditary spastic paraplegia. Brain *145*, 3095. 10.1093/BRAIN/AWAC123.

39. Omotade, O.F., Rui, Y., Lei, W., Yu, K., Hartzell, H.C., Fowler, V.M., and Zheng, J.Q. (2018). Tropomodulin Isoform-Specific Regulation of Dendrite Development and Synapse Formation. The Journal of Neuroscience *38*, 10271. 10.1523/JNEUROSCI.3325-17.2018.

40. Bräuer, A.U., Savaskan, N.E., Kühn, H., Prehn, S., Ninnemann, O., and Nitsch, R. (2003). A new phospholipid phosphatase, PRG-1, is involved in axon growth and regenerative sprouting. Nature Neuroscience 2003 6:6 *6*, 572–578. 10.1038/nn1052.

41. Yu, Q.S., Feng, W.Q., Shi, L.L., Niu, R.Z., and Liu, J. (2022). Integrated Analysis of Cortex Single-Cell Transcriptome and Serum Proteome Reveals the Novel Biomarkers in Alzheimer's Disease. Brain Sciences *12*. 10.3390/BRAINSCI12081022/S1.

42. Zito, A., Cartelli, D., Cappelletti, G., Cariboni, A., Andrews, W., Parnavelas, J., Poletti, A., and Galbiati, M. (2014). Neuritin 1 promotes neuronal migration. Brain Structure and Function *219*, 105–118. 10.1007/S00429-012-0487-1/FIGURES/6.

43. Wanigasekara, Y., Airaksinen, M.S., Heuckeroth, R.O., Milbrandt, J., and Keast, J.R. (2004). Neurturin signalling via GFRα2 is essential for innervation of glandular but not muscle targets of sacral parasympathetic ganglion neurons. Molecular and Cellular Neuroscience *25*, 288–300. 10.1016/J.MCN.2003.10.019.

44. Kessi, M., Chen, B., Peng, J., Yan, F., Yang, L., and Yin, F. (2021). Calcium channelopathies and intellectual disability: a systematic review. Orphanet Journal of Rare Diseases *16*. 10.1186/S13023-021-01850-0.

45. Smith, R.S., Kenny, C.J., Ganesh, V., Jang, A., Borges-Monroy, R., Partlow, J.N., Hill, R.S., Shin, T., Chen, A.Y., Doan, R.N., et al. (2018). Sodium Channel SCN3A (NaV1.3) Regulation of Human Cerebral Cortical Folding and Oral Motor Development. Neuron *99*, 905-913.e7. 10.1016/J.NEURON.2018.07.052.

46. La Manno, G., Gyllborg, D., Codeluppi, S., Nishimura, K., Salto, C., Zeisel, A., Borm, L.E., Stott, S.R.W., Toledo, E.M., Villaescusa, J.C., et al. (2016). Molecular Diversity of Midbrain Development in Mouse, Human, and Stem Cells. Cell *167*, 566-580.e19. 10.1016/J.CELL.2016.09.027.

47. Hou, P.S., hAilín, D., Vogel, T., and Hanashima, C. (2020). Transcription and Beyond: Delineating FOXG1 Function in Cortical Development and Disorders. Frontiers in Cellular Neuroscience *14*. 10.3389/FNCEL.2020.00035.

48. Méndez-Maldonado, K., Vega-López, G.A., Aybar, M.J., and Velasco, I. (2020). Neurogenesis From Neural Crest Cells: Molecular Mechanisms in the Formation of Cranial Nerves and Ganglia. Frontiers in Cell and Developmental Biology *8*. 10.3389/FCELL.2020.00635.

49. Zhang, Z.H., and Song, G.L. (2021). Roles of Selenoproteins in Brain Function and the Potential Mechanism of Selenium in Alzheimer's Disease. Frontiers in Neuroscience *15*. 10.3389/FNINS.2021.646518.

50. Aiken, J., Buscaglia, G., Bates, E.A., and Moore, J.K. (2017). The α-Tubulin gene TUBA1A in Brain Development: A Key Ingredient in the Neuronal Isotype Blend. Journal of Developmental Biology *5*. 10.3390/JDB5030008.

51. Leandro-García, L.J., Leskelä, S., Landa, I., Montero-Conde, C., López-Jiménez, E., Letón, R., Cascón, A., Robledo, M., and Rodríguez-Antona, C. (2010). Tumoral and tissue-specific expression of the major human β-tubulin isotypes. Cytoskeleton *67*, 214–223. 10.1002/CM.20436.

52. Zhao, Z., Zhang, D., Yang, F., Xu, M., Zhao, S., Pan, T., Liu, C., Liu, Y., Wu, Q., Tu, Q., et al. (2022). Evolutionarily conservative and non-conservative regulatory networks during primate interneuron development revealed by single-cell RNA and ATAC sequencing. Cell Research *32*, 425. 10.1038/S41422-022-00635-9.

53. Granja, J.M., Corces, M.R., Pierce, S.E., Bagdatli, S.T., Choudhry, H., Chang, H.Y., and Greenleaf, W.J. (2021). ArchR is a scalable software package for integrative single-cell chromatin accessibility analysis. Nature Genetics *53*, 403–411. 10.1038/s41588-021-00790-6.

54. Ogryzko, V. V., Schiltz, R.L., Russanova, V., Howard, B.H., and Nakatani, Y. (1996). The transcriptional coactivators p300 and CBP are histone acetyltransferases. Cell *87*, 953–959. 10.1016/S0092-8674(00)82001-2.

55. Lan, F., Bayliss, P.E., Rinn, J.L., Whetstine, J.R., Wang, J.K., Chen, S., Iwase, S., Alpatov, R., Issaeva, I., Canaani, E., et al. (2007). A histone H3 lysine 27 demethylase regulates animal posterior development. Nature 2007 449:7163 *449*, 689–694. 10.1038/nature06192.

56. Adra, C.N., Donato, J.L., Badovinac, R., Syed, F., Kheraj, R., Cai, H., Moran, C., Kolker, M.T., Turner, H., Weremowicz, S., et al. (2000). SMARCAD1, a Novel Human Helicase Family-Defining Member Associated with Genetic Instability: Cloning, Expression, and Mapping to 4q22–q23, a Band Rich in Breakpoints and Deletion Mutants Involved in Several Human Diseases. Genomics *69*, 162–173. 10.1006/GENO.2000.6281.

57. Baizabal, J.M., Mistry, M., García, M.T., Gómez, N., Olukoya, O., Tran, D., Johnson, M.B., Walsh, C.A., and Harwell, C.C. (2018). The Epigenetic State of PRDM16-Regulated Enhancers in Radial Glia Controls Cortical Neuron Position. Neuron *98*, 945-962.e8. 10.1016/J.NEURON.2018.04.033.

58. Mao, Y., and Lee, A.W.M. (2005). A novel role for Gab2 in bFGF-mediated cell survival during retinoic acid–induced neuronal differentiation. The Journal of Cell Biology *170*, 305. 10.1083/JCB.200505061.

59. Louvi, A., and Artavanis-Tsakonas, S. (2006). Notch signalling in vertebrate neural development. Nature Reviews Neuroscience 2006 7:2 *7*, 93–102. 10.1038/nrn1847.

60. Holtz, A.M., Peterson, K.A., Nishi, Y., Morin, S., Song, J.Y., Charron, F., Mcmahon, A.P., and Allen, B.L. (2013). Essential role for ligand-dependent feedback antagonism of vertebrate hedgehog signaling by PTCH1, PTCH2 AND HHIP1 during neural patterning. Development (Cambridge) *140*, 3423–3434. 10.1242/DEV.095083/-/DC1.

61. Onishi, K., and Zou, Y. (2017). Sonic Hedgehog switches on Wnt/planar cell polarity signaling in commissural axon growth cones by reducing levels of Shisa2. eLife *6*. 10.7554/ELIFE.25269.

62. Sanders, S.S., Hernandez, L.M., Soh, H., Karnam, S., Walikonis, R.S., Tzingounis, A. V., and Thomas, G.M. (2020). The palmitoyl acyltransferase ZDHHC14 controls Kv1-family potassium channel clustering at the axon initial segment. eLife *9*, 1–32. 10.7554/ELIFE.56058.

63. Imaizumi, K., Tsuda, M., Wanaka, A., Tohyama, M., and Takagi, T. (1994). Differential expression of sgk mRNA, a member of the Ser/Thr protein kinase gene family, in rat brain after CNS injury. Molecular Brain Research *26*, 189–196. 10.1016/0169-328X(94)90090-6.

64. Pietzsch, A., Büchler, C., and Schmitz, G. (1998). Genomic Organization, Promoter Cloning, and Chromosomal Localization of the Dif-2 Gene. Biochemical and Biophysical Research Communications *245*, 651–657. 10.1006/BBRC.1998.8500.

65. Lim, F.T., Ogawa, S., and Parhar, I.S. (2016). Spred-2 expression is associated with neural repair of injured adult zebrafish brain. Journal of Chemical Neuroanatomy *77*, 176–186. 10.1016/J.JCHEMNEU.2016.07.005.

66. Yosten, G.L.C., Harada, C.M., Haddock, C., Giancotti, L.A., Kolar, G.R., Patel, R., Guo, C., Chen, Z., Zhang, J., Doyle, T.M., et al. (2020). GPR160 de-orphanization reveals critical roles in neuropathic pain in rodents. The Journal of Clinical Investigation *130*, 2587. 10.1172/JCI133270.

67. Bennett, K.M., Liu, J., Hoelting, C., and Stoll, J. (2011). Expression and analysis of two novel rat organic cation transporter homologs, SLC22A17 and SLC22A23. Molecular and cellular biochemistry *352*, 143. 10.1007/S11010-011-0748-Y.

68. Demontis, D., Walters, R.K., Martin, J., Mattheisen, M., Als, T.D., Agerbo, E., Baldursson, G., Belliveau, R., Bybjerg-Grauholm, J., Bækvad-Hansen, M., et al. (2019). Discovery of the first genome-wide significant risk loci for attention deficit/hyperactivity disorder. Nature Genetics *51*, 63–75. 10.1038/s41588-018-0269-7.

69. Sekaninova, N., Mestanik, M., Mestanikova, A., Hamrakova, A., and Tonhajzerova, I. (2019). Novel Approach to Evaluate Central Autonomic Regulation in Attention Deficit/Hyperactivity Disorder (ADHD). 10.33549/physiolres.934160.

70. Morris, S.S.J., Musser, E.D., Tenenbaum, R.B., Ward, A.R., Martinez, J., Raiker, J.S., Coles, E.K., and Riopelle, C. (2020). Emotion Regulation via the Autonomic Nervous System in Children with Attention-Deficit/Hyperactivity Disorder (ADHD): Replication and Extension. Journal of abnormal child psychology *48*, 361. 10.1007/S10802-019-00593-8.

71. Griffiths, K.R., Quintana, D.S., Hermens, D.F., Spooner, C., Tsang, T.W., Clarke, S., and Kohn, M.R. (2017). Sustained attention and heart rate variability in children and adolescents with ADHD. Biological Psychology *124*, 11–20. 10.1016/j.biopsycho.2017.01.004.

72. Montalbán-Loro, R., Lassi, G., Lozano-Ureña, A., Perez-Villalba, A., Jiménez-Villalba, E., Charalambous, M., Vallortigara, G., Horner, A.E., Saksida, L.M., Bussey, T.J., et al. (2021). Dlk1 dosage regulates hippocampal neurogenesis and cognition. Proceedings of the National Academy of Sciences of the United States of America *118*. 10.1073/PNAS.2015505118/-/DCSUPPLEMENTAL.

73. Tang, J., Yu, Y., and Yang, W. (2017). Long noncoding RNA and its contribution to autism spectrum disorders. CNS Neuroscience & Therapeutics *23*, 645. 10.1111/CNS.12710.

74. Zayats, T., Johansson, S., and Haavik, J. (2015). Expanding the toolbox of ADHD genetics. How can we make sense of parent of origin effects in ADHD and related behavioral phenotypes? Behavioral and Brain Functions : BBF *11*, 33. 10.1186/S12993-015-0078-4.

75. Shimada, I.S., Acar, M., Burgess, R.J., Zhao, Z., and Morrison, S.J. (2017). Prdm16 is required for the maintenance of neural stem cells in the postnatal forebrain and their differentiation into ependymal cells. Genes and Development *31*, 1134–1146. 10.1101/GAD.291773.116/-/DC1.

76. Creyghton, M.P., Cheng, A.W., Welstead, G.G., Kooistra, T., Carey, B.W., Steine, E.J., Hanna, J., Lodato, M.A., Frampton, G.M., Sharp, P.A., et al. (2010). Histone H3K27ac separates active from poised enhancers and predicts developmental state. Proceedings of the National Academy of Sciences of the United States of America *107*, 21931–21936. 10.1073/PNAS.1016071107/SUPPL_FILE/ST01.XLSX.

77. Kaiser, A., Broeder, C., Cohen, J.R., Douw, L., Reneman, L., and Schrantee, A. (2022). Effects of a single-dose methylphenidate challenge on resting-state functional connectivity in

stimulant-treatment naive children and adults with ADHD. Human Brain Mapping *43*, 4664. 10.1002/HBM.25981.

78. Grimm, O., Thomä, L., Kranz, T.M., and Reif, A. (2022). Is genetic risk of ADHD mediated via dopaminergic mechanism? A study of functional connectivity in ADHD and pharmacologically challenged healthy volunteers with a genetic risk profile. Translational Psychiatry *12*. 10.1038/S41398-022-02003-Y.

79. El Amine, F., Heidinger, B., Cameron, J.D., Hafizi, K., Banifatemi, S., Robaey, P., Vaillancourt, R., Goldfield, G.S., and Doucet, E. (2022). Two-month administration of methylphenidate improves olfactory sensitivity and suppresses appetite in individuals with obesity. Canadian Journal of Physiology and Pharmacology *100*, 432–440. 10.1139/CJPP-2021-0318/ASSET/IMAGES/CJPP-2021-0318TAB2.GIF.

80. Yuan, D., Zhang, M., Huang, Y., Wang, X., Jiao, J., and Huang, Y. (2021). Noradrenergic genes polymorphisms and response to methylphenidate in children with ADHD: A systematic review and meta-analysis. Medicine *100*, e27858. 10.1097/MD.0000000000027858.

81. Bjørk, M.H., Zoega, H., Leinonen, M.K., Cohen, J.M., Dreier, J.W., Furu, K., Gilhus, N.E., Gissler, M., Hálfdánarson, Ó., Igland, J., et al. (2022). Association of Prenatal Exposure to Antiseizure Medication With Risk of Autism and Intellectual Disability. JAMA Neurology *79*, 672–681. 10.1001/JAMANEUROL.2022.1269.

82. Goasdoué, K., Miller, S.M., Colditz, P.B., and Björkman, S.T. (2017). Review: The blood-brain barrier; protecting the developing fetal brain. Placenta *54*, 111–116. 10.1016/J.PLACENTA.2016.12.005.

83. Addo, K.A., Bulka, C., Dhingra, R., Santos, H.P., Smeester, L., O'Shea, T.M., and Fry, R.C. (2019). Acetaminophen use during pregnancy and DNA methylation in the placenta of the extremely low gestational age newborn (ELGAN) cohort. Environmental Epigenetics *5*, 1–10. 10.1093/eep/dvz010.

84. Olstad, E.W., Nordeng, H.M.E., and Gervin, K. (2021). Prenatal medication exposure and epigenetic outcomes: a systematic literature review and recommendations for prenatal pharmacoepigenetic studies. Epigenetics, 1–24. 10.1080/15592294.2021.1903376.

85. Eslamimehr, S., Jones, A.D., Anthony, T.M., Arshad, S.H., Holloway, J.W., Ewart, S., Luo, R., Mukherjee, N., Kheirkhah Rahimabad, P., Chen, S., et al. (2022). Association of prenatal acetaminophen use and acetaminophen metabolites with DNA methylation of newborns: analysis of two consecutive generations of the Isle of Wight birth cohort. Environmental Epigenetics *8*, 1–10. 10.1093/EEP/DVAC002.

86. Ström, S., Holm, F., Bergström, R., Strömberg, A.M., and Hovatta, O. (2010). Derivation of 30 human embryonic stem cell lines—improving the quality. In Vitro Cellular & Developmental Biology. Animal *46*, 337. 10.1007/S11626-010-9308-0.

87. Ávila-González, D., Portillo, W., García-López, G., Molina-Hernández, A., Díaz-Martínez, N.E., and Díaz, N.F. (2021). Unraveling the Spatiotemporal Human Pluripotency in Embryonic Development. Frontiers in Cell and Developmental Biology *9*. 10.3389/FCELL.2021.676998.

88. Ahokas, R.A., and McKinney, E.T. (2009). Development and Physiology of the Placenta and Membranes (Sapiens Publishing, LTD) 10.3843/GLOWM.10101.

89. Conings, S., Tseke, F., Van Den Broeck, A., Qi, B., Paulus, J., Amant, F., Annaert, P., and Van Calsteren, K. (2019). Transplacental transport of paracetamol and its phase II metabolites using the ex vivo placenta perfusion model. 10.1016/j.taap.2019.03.004.

90. Hodyl, N.A., Roberts, C.T., and Bianco-Miotto, T. (2016). Cord Blood DNA Methylation Biomarkers for Predicting Neurodevelopmental Outcomes. Genes *7*, 117. 10.3390/genes7120117.

91. Cortes, D., and Pera, M.F. (2021). The genetic basis of inter-individual variation in recovery from traumatic brain injury. npj Regenerative Medicine 2021 6:1 *6*, 1–9. 10.1038/S41536-020-00114-Y.

92. Finno, C.J., Chen, Y., Park, S., Lee, J.H., Perez-Flores, M.C., Choi, J., and Yamoah, E.N. (2022). Cisplatin Neurotoxicity Targets Specific Subpopulations and K+ Channels in Tyrosine-Hydroxylase Positive Dorsal Root Ganglia Neurons. Frontiers in Cellular Neuroscience *16*. 10.3389/FNCEL.2022.853035/FULL.

93. Jayanthi, S., Daiwile, A.P., and Cadet, J.L. (2021). Neurotoxicity of methamphetamine: main effects and mechanisms. Experimental neurology *344*, 113795. 10.1016/J.EXPNEUROL.2021.113795.

94. Gervin, K., Nordeng, H., Ystrom, E., Reichborn-Kjennerud, T., and Lyle, R. (2017). Long-term prenatal exposure to paracetamol is associated with DNA methylation differences in children diagnosed with ADHD. Clin Epigenetics *9*, 345. 10.1186/s13148-017-0376-9.

95. Thapa, D., Wu, K., Stoner, M.W., Xie, B., Zhang, M., Manning, J.R., Lu, Z., Li, J.H., Chen, Y., Gucek, M., et al. (2018). The protein acetylase GCN5L1 modulates hepatic fatty acid oxidation activity via acetylation of the mitochondrial β-oxidation enzyme HADHA. The Journal of Biological Chemistry *293*, 17676. 10.1074/JBC.AC118.005462.

96. Schroeder, B.C., Waldegger, S., Fehr, S., Bleich, M., Warth, R., Greger, R., and Jentsch, T.J. (2000). A constitutively open potassium channel formed by KCNQ1 and KCNE3. Nature 2000 403:6766 *403*, 196–199. 10.1038/35003200.

97. Miura, R., Araki, A., Minatoya, M., Miyake, K., Chen, M.L., Kobayashi, S., Miyashita, C., Yamamoto, J., Matsumura, T., Ishizuka, M., et al. (2019). An epigenome-wide analysis of cord blood DNA methylation reveals sex-specific effect of exposure to bisphenol A. Scientific Reports *9*, 1–13. 10.1038/s41598-019-48916-5.

98. Koehn, L.M., Huang, Y., Habgood, M.D., Nie, S., Chiou, S.Y., Banati, R.B., Dziegielewska, K.M., and Saunders, N.R. (2021). Efflux transporters in rat placenta and developing brain: transcriptomic and functional response to paracetamol. Scientific Reports *11*. 10.1038/S41598-021-99139-6.

99. Koenderink, J.B., van den Heuvel, J.J.M.W., Bilos, A., Vredenburg, G., Vermeulen, N.P.E., and Russel, F.G.M. (2020). Human multidrug resistance protein 4 (MRP4) is a cellular efflux transporter for paracetamol glutathione and cysteine conjugates. Archives of Toxicology *94*, 3027. 10.1007/S00204-020-02793-4.

100. Koehn, L.M., Huang, Y., Habgood, M.D., Kysenius, K., Crouch, P.J., Dziegielewska, K.M., and Saunders, N.R. (2020). Effects of paracetamol (acetaminophen) on gene expression and permeability properties of the rat placenta and fetal brain. F1000Res *9*. 10.12688/f1000research.24119.2.

101. Mahley, R.W., and Huang, Y. (2012). Apolipoprotein E Sets the Stage: Response to Injury Triggers Neuropathology, Including Alzheimer's Disease. Neuron *76*, 871. 10.1016/J.NEURON.2012.11.020.

102. Malik, A.R., and Willnow, T.E. (2019). Excitatory Amino Acid Transporters in Physiology and Disorders of the Central Nervous System. International Journal of Molecular Sciences *20*. 10.3390/IJMS20225671.

103. Tüshaus, J., Müller, S.A., Kataka, E.S., Zaucha, J., Monasor, L.S., Su, M., Güner, G., Jocher, G., Tahirovic, S., Frishman, D., et al. (2020). An optimized quantitative proteomics method establishes the cell type-resolved mouse brain secretome. The EMBO Journal *39*. 10.15252/EMBJ.2020105693.

104. Ouyang, J.F., Kamaraj, U.S., Cao, E.Y., and Rackham, O.J.L. (2021). ShinyCell: simple and sharable visualization of single-cell gene expression data. Bioinformatics *37*, 3374–3376. 10.1093/BIOINFORMATICS/BTAB209.

105. Sharma, A., Akshay, A., Rogne, M., and Eskeland, R. (2022). ShinyArchR.UiO: user-friendly,integrative and open-source tool for visualization of single-cell ATAC-seq data using ArchR. Bioinformatics *38*, 834–836. 10.1093/BIOINFORMATICS/BTAB680.

106. Samara, A., Spildrejorde, M., Sharma, A., Falck, M., Leithaug, M., Modafferi, S., Bjørnstad, P.M., Acharya, G., Gervin, K., Lyle, R., et al. (2022). A multi-omics approach to visualize early neuronal differentiation from hESCs in 4D. iScience *25*, 105279. 10.1016/j.isci.2022.105279.

107. R Core Team (2019). A Language and Environment for Statistical Computing. R Foundation for Statistical Computing.

108. Hao, Y., Hao, S., Andersen-Nissen, E., Mauck, W.M., Zheng, S., Butler, A., Lee, M.J., Wilk, A.J., Darby, C., Zager, M., et al. (2021). Integrated analysis of multimodal single-cell data. Cell *184*, 3573-3587.e29. 10.1016/j.cell.2021.04.048.

109. Stuart, T., Butler, A., Hoffman, P., Hafemeister, C., Papalexi, E., Mauck, W.M., Hao, Y., Stoeckius, M., Smibert, P., and Satija, R. (2019). Comprehensive Integration of Single-Cell Data. Cell *177*, 1888-1902.e21. 10.1016/j.cell.2019.05.031.

110. Stuart, T., Srivastava, A., Madad, S., Lareau, C.A., and Satija, R. (2021). Single-cell chromatin state analysis with Signac. Nat Methods *18*, 1333–1341. 10.1038/s41592-021-01282-5.

111. Pagès, H. (2020). BSgenome: Software infrastructure for efficient representation of full genomes and their SNPs version 1.58.0 from Bioconductor. https://rdrr.io/bioc/BSgenome/.

112. Ouyang, J.F., Kamaraj, U.S., Cao, E.Y., and Rackham, O.J.L. (2021). ShinyCell: simple and sharable visualization of single-cell gene expression data. Bioinformatics. 10.1093/bioinformatics/btab209.

113. Sharma, A., Akshay, A., Rogne, M., and Eskeland, R. (2021). ShinyArchR.UiO: user-friendly, integrative and open-source tool for visualization of single-cell ATAC-seq data using ArchR. Bioinformatics. 10.1093/bioinformatics/btab680.

114. Gulati, G.S., Sikandar, S.S., Wesche, D.J., Manjunath, A., Bharadwaj, A., Berger, M.J., Ilagan, F., Kuo, A.H., Hsieh, R.W., Cai, S., et al. (2020). Single-cell transcriptional diversity is a hallmark of developmental potential. Science. 10.1126/science.aax0249.

115. The Bioconductor Dev Team (2021). BSgenome.Hsapiens.UCSC.hg38. Bioconductor. http://bioconductor.org/packages/BSgenome.Hsapiens.UCSC.hg38/.

116. Rainer, J. (2017). EnsDb.Hsapiens.v86. Bioconductor. http://bioconductor.org/packages/EnsDb.Hsapiens.v86/.

117. Zappia, L., and Oshlack, A. (2018). Clustering trees: a visualization for evaluating clusterings at multiple resolutions. GigaScience *7*. 10.1093/gigascience/giy083.

118. McCarthy, D.J., Campbell, K.R., Lun, A.T.L., and Wills, Q.F. (2017). Scater: pre-processing, quality control, normalization and visualization of single-cell RNA-seq data in R. Bioinformatics *33*, 1179–1186. 10.1093/bioinformatics/btw777.

119. Love, M.I., Huber, W., and Anders, S. (2014). Moderated estimation of fold change and dispersion for RNA-seq data with DESeq2. Genome Biol. *15*, 550. 10.1186/s13059-014-0550-8.

120. Subramanian, A., Tamayo, P., Mootha, V.K., Mukherjee, S., Ebert, B.L., Gillette, M.A., Paulovich, A., Pomeroy, S.L., Golub, T.R., Lander, E.S., et al. (2005). Gene set enrichment analysis: A knowledge-based approach for interpreting genome-wide expression profiles. PNAS *102*, 15545–15550. 10.1073/pnas.0506580102.

121. Aryee, M.J., Jaffe, A.E., Corrada-Bravo, H., Ladd-Acosta, C., Feinberg, A.P., Hansen, K.D., and Irizarry, R.A. (2014). Minfi: a flexible and comprehensive Bioconductor package for the analysis of Infinium DNA methylation microarrays. Bioinformatics *30*, 1363–1369. 10.1093/bioinformatics/btu049.

122. Ritchie, M.E., Phipson, B., Wu, D., Hu, Y., Law, C.W., Shi, W., and Smyth, G.K. (2015). limma powers differential expression analyses for RNA-sequencing and microarray studies. Nucleic Acids Res *43*, e47. 10.1093/nar/gkv007.

123. Ren, X., and Kuan, P.F. (2019). methylGSA: a Bioconductor package and Shiny app for DNA methylation data length bias adjustment in gene set testing. 10.1093/bioinformatics/bty892.

124. Aran, D., Looney, A.P., Liu, L., Wu, E., Fong, V., Hsu, A., Chak, S., Naikawadi, R.P., Wolters, P.J., Abate, A.R., et al. (2019). Reference-based analysis of lung single-cell sequencing reveals a transitional profibrotic macrophage. Nat Immunol *20*, 163–172. 10.1038/s41590-018-0276-y.

125. Korsunsky, I., Millard, N., Fan, J., Slowikowski, K., Zhang, F., Wei, K., Baglaenko, Y., Brenner, M., Loh, P., and Raychaudhuri, S. (2019). Fast, sensitive and accurate integration of single-cell data with Harmony. Nat Methods *16*, 1289–1296. 10.1038/s41592-019-0619-0.

126. McLean, C.Y., Bristor, D., Hiller, M., Clarke, S.L., Schaar, B.T., Lowe, C.B., Wenger, A.M., and Bejerano, G. (2010). GREAT improves functional interpretation of cis-regulatory regions. Nat Biotech *28*, 495–501. 10.1038/nbt.1630.

127. Khan, A., and Mathelier, A. (2017). Intervene: a tool for intersection and visualization of multiple gene or genomic region sets. BMC Bioinformatics *18*, 287. 10.1186/s12859-017-1708-7.

128. Kolberg, L., Raudvere, U., Kuzmin, I., Vilo, J., and Peterson, H. (2020). gprofiler2 -- an R package for gene list functional enrichment analysis and namespace conversion toolset g:Profiler. 10.12688/f1000research.24956.2.

129. Feng, J., Liu, T., Qin, B., Zhang, Y., and Liu, X.S. (2012). Identifying ChIP-seq enrichment using MACS. Nat Protoc *7*, 1728–1740. 10.1038/nprot.2012.101.

130. Bryne, J.C., Valen, E., Tang, M.-H.E., Marstrand, T., Winther, O., da Piedade, I., Krogh, A., Lenhard, B., and Sandelin, A. (2008). JASPAR, the open access database of transcription factor-binding profiles: new content and tools in the 2008 update. Nucleic Acids Res *36*, D102-6. 10.1093/nar/gkm955.

131. Amezquita, R.A., Lun, A.T.L., Becht, E., Carey, V.J., Carpp, L.N., Geistlinger, L., Marini, F., Rue-Albrecht, K., Risso, D., Soneson, C., et al. (2020). Orchestrating single-cell analysis with Bioconductor. Nat Methods *17*, 137–145. 10.1038/s41592-019-0654-x.

132. Borcherding, N., and Andrews, J. (2022). escape: Easy single cell analysis platform for enrichment. 10.18129/B9.bioc.escape.

133. Garnier, S., Ross, N., Camargo, A.P., Rudis, boB, and Woo, K. (2021). sjmgarnier/viridisLite: CRAN release v0.4.0. 10.5281/zenodo.4686664.

134. Ge, S.X., Jung, D., and Yao, R. (2020). ShinyGO: a graphical gene-set enrichment tool for animals and plants. Bioinformatics *36*, 2628–2629. 10.1093/bioinformatics/btz931.

135. Van Rossum, G., and Drake, F.L. (2009). Python 3 Reference Manual. (Scotts Valley, CA: CreateSpace.).

136. Gu, Z., Eils, R., and Schlesner, M. (2016). Complex heatmaps reveal patterns and correlations in multidimensional genomic data. Bioinformatics *32*, 2847–2849. 10.1093/bioinformatics/btw313.

137. Gu, Z. (2022). Complex heatmap visualization. iMeta *1*, e43. 10.1002/imt2.43.

138. Wickham, H. (2009). ggplot2: Elegant Graphics for Data Analysis (Springer-Verlag) 10.1007/978-0-387-98141-3.

139. Lawrence, M., Huber, W., Pagès, H., Aboyoun, P., Carlson, M., Gentleman, R., Morgan, M.T., and Carey, V.J. (2013). Software for Computing and Annotating Genomic Ranges. PLOS Computational Biology *9*, e1003118. 10.1371/journal.pcbi.1003118.

140. Wickham, H., Averick, M., Bryan, J., Chang, W., McGowan, L.D., François, R., Grolemund, G., Hayes, A., Henry, L., Hester, J., et al. (2019). Welcome to the Tidyverse. Journal of Open Source Software *4*, 1686. 10.21105/joss.01686.

141. Kassambara, A. (2020). ggpubr: “ggplot2” Based Publication Ready Plots.

142. Varet, H., Brillet-Guéguen, L., Coppée, J.-Y., and Dillies, M.-A. (2016). SARTools: A DESeq2- and EdgeR-Based R Pipeline for Comprehensive Differential Analysis of RNA-Seq Data. PLOS ONE *11*, e0157022. 10.1371/journal.pone.0157022.

143. Main, H., Hedenskog, M., Acharya, G., Hovatta, O., and Lanner, F. (2020). Karolinska Institutet Human Embryonic Stem Cell Bank. Stem Cell Research *45*, 101810. 10.1016/j.scr.2020.101810.

144. Nitsche, J., Patil, A., Langman, L., Penn, H., Derleth, D., Watson, W., and Brost, B. (2017). Transplacental Passage of Acetaminophen in Term Pregnancy. American Journal of Perinatology *34*, 541–543. 10.1055/s-0036-1593845.

145. Bannwarth, B., Netter, P., Lapicque, F., Gillet, P., Pere, P., Boccard, E., Royer, R., and Gaucher, A. (1992). Plasma and cerebrospinal fluid concentrations of paracetamol after a single intravenous dose of propacetamol. British Journal of Clinical Pharmacology *34*, 79. 10.1111/J.1365-2125.1992.TB04112.X.

146. Anderson, B.J., Holford, N.H.G., Woollard, G.A., and Chan, P.L.S. (1998). Paracetamol plasma and cerebrospinal fluid pharmacokinetics in children. British Journal of Clinical Pharmacology *46*, 237–243. 10.1046/j.1365-2125.1998.00780.x.

147. Kumpulainen, E., Kokki, H., Halonen, T., Heikkinen, M., Savolainen, J., and Laisalmi, M. (2007). Paracetamol (acetaminophen) penetrates readily into the cerebrospinal fluid of children after intravenous administration. Pediatrics *119*, 766–771. 10.1542/peds.2006-3378.

148. Coulter, S.J. (2018). Mitigation of the effect of variability in digital PCR assays through use of duplexed reference assays for normalization. BioTechniques *65*, 86–91. 10.2144/btn-2018-0058.

149. Bushnell, B. (2014). BBMap: A Fast, Accurate, Splice-Aware Aligner.

150. Kim, D., Langmead, B., and Salzberg, S.L. (2015). HISAT: A fast spliced aligner with low memory requirements. Nature Methods *12*, 357–360. 10.1038/nmeth.3317.

151. Liao, Y., Smyth, G.K., and Shi, W. (2014). FeatureCounts: An efficient general purpose program for assigning sequence reads to genomic features. Bioinformatics *30*, 923–930. 10.1093/bioinformatics/btt656.

152. R Core Team (2021). R: A language and environment for statistical computing.

153. Love, M.I., Huber, W., and Anders, S. (2014). Moderated estimation of fold change and dispersion for RNA-seq data with DESeq2. Genome Biology *15*, 550. 10.1186/s13059-014-0550-8.

154. Kolde, R. (2019). pheatmap: Pretty Heatmaps.

155. Triche, T.J., Weisenberger, D.J., Van Den Berg, D., Laird, P.W., and Siegmund, K.D. (2013). Low-level processing of Illumina Infinium DNA Methylation BeadArrays. Nucleic Acids Research *41*, e90. 10.1093/nar/gkt090.

156. Fortin, J.P., Labbe, A., Lemire, M., Zanke, B.W., Hudson, T.J., Fertig, E.J., Greenwood, C.M.T., and Hansen, K.D. (2014). Functional normalization of 450k methylation array data improves replication in large cancer studies. Genome Biology *15*, 503. 10.1186/s13059-014-0503-2.

157. Hafemeister, C., and Satija, R. (2019). Normalization and variance stabilization of single-cell RNA-seq data using regularized negative binomial regression. Genome Biology *20*, 296. 10.1186/s13059-019-1874-1.

158. Tirosh, I., Izar, B., Prakadan, S.M., Wadsworth, M.H., Treacy, D., Trombetta, J.J., Rotem, A., Rodman, C., Lian, C., Murphy, G., et al. (2016). Dissecting the multicellular ecosystem of metastatic melanoma by single-cell RNA-seq. Science *352*, 189–196. 10.1126/science.aad0501.

159. Risso, D., and Cole, M. (2022). scRNAseq: Collection of Public Single-Cell RNA-Seq Datasets.